Properties of the spectral response cost functional employed in the inverse wave-scattering problem of the retrieval of the shear body wavespeed of the homogeneous solid occupying a half space bounded by a plane stress-free surface

Thierry Scotti, Armand Wirgin

Properties of the spectral response cost functional employed in the inverse wave-scattering problem of the retrieval of the shear body wavespeed of the homogeneous solid occupying a half space bounded by a plane stress-free surface

Thierry Scotti* and Armand Wirgin†

August 14, 2015

Abstract

Parseval's theorem leads to the finding that the minima of a least-squares spectral response cost functional K are at the same positions as the minima of a least squares signal response functional C. We describe the useful functional properties of K, in the context of a simple geophysical inverse problem pertaining to the retrieval of the shear wavespeed in a homogeneous underground, notably for enabling the location of its global minimum and dealing with the secondary minima. We show how the width of the search interval, the number and positions of the sensors, as well as the central frequency and bandwidth of the spectrum of the probe radiation, condition the aspect of the cost functional, particularly as regards the number of secondary minima and the depth of the trough associated with the global minimum. Finally, we evaluate the influence of prior uncertainties on the accuracy of the retrieval (via K) of the shear body wavespeed of the underground.

keywords: inverse theory, acoustic properties, body waves, seismic tomography

section: seismology

*scotti@lma.cnrs-mrs.fr, LMA, CNRS, UPR 7051, Aix-Marseille Univ, Centrale Marseille, F-13402 Marseille Cedex 20, France

†wirgin@lma.cnrs-mrs.fr, LMA, CNRS, UPR 7051, Aix-Marseille Univ, Centrale Marseille, F-13402 Marseille Cedex 20, France

Contents

1 Introduction

Many seismic inverse problems (IP) consist in retrieving a set of parameters of the seismic source and/or of the medium traversed by the wave emitted from the source. These IP involve two indispensable ingredients: 1) the signals (hereafter termed: *data*) recorded by sensors located on/underneath the boundary (e.g., the ground, often assumed to be flat) constituting the response of the medium to the wave and 2) a theoretical model (hereafter termed: *retrieval model*) of how such a response can be produced.

The sought-for parameters form a subset $\mathbf{R}$ of the set of parameters $\mathbf{P}$ inherent in the retrieval model and the remaining parameters (hereafter termed: priors), forming the set $\mathbf{Q}$, are considered to be known (which simply means that no effort is made to retrieve them in the given IP). The inversion consists in extracting $\mathbf{R}$ from the retrieval model by comparing the latter to the data [11]. Thus, the retrieved $\mathbf{R}$ is usually considered to be the set that yields the best fit between the response data and the prediction of this response furnished by the retrieval model.

Often, the notion of best fit is synonymous with the attainment of the *global minimum* of a L_2 cost functional involving the square of the absolute difference the predicted response and the actual response. The response can either take its "natural" space-time form, or its space-frequency form; in the first eventuality, the cost functional C involves temporal integrals of squared (real) response differences whereas in the second eventuality, the cost functional K involves frequency integrals of absolute squared (complex) response differences. In either case, to get a full grasp of the complexities involved in seismic IP, one must obtain an adequate representation of the (preferably-mathematical) properties of the cost functional.

If the number of parameters of $\mathbf{R}$ exceeds two, it becomes impossible to obtain a complete graphical representation of C or K; in this situation, either graphs of the cost versus one or two parameters at a time are offered [4, 2, 14, 8, 10] or the properties of the cost functionals are studied in rather abstract terms [7]. Non-uniqueness is often evoked as being an essential aspect of the ill-posed character of IP [9]), but cases are also encountered in which either the solution of the IP is sought (by employing local search algorithms) as if it were unique or cost functionals are obtained which appear to be convex in the search domain of $\mathbf{R}$ [13, 8, 14]: is this apparent uniqueness due to the choice of space-time rather than space-frequency cost functionals, to the choice of a rather small search domain, or to some other cause?. More generally, the question arises as to how to interpret a cost functional that possesses a single, relatively-deep minimum and several relatively-shallow minima [3, 2, 14, 6]: is this the consequence of errors or bad choices in the recording and processing of data and/or of the choice of retrieval model, and/or due to some other cause such as uncertainty of the values ascribed to the priors in the set $\mathbf{Q}$? It is difficult to provide rational answers to such questions in the usually-encountered seismic inverse problems which involve many to-be-retrieved parameters and mathematically (and/or numerically)-elaborate retrieval models. This is why it appears to be opportune to focus attention on a seismic IP involving the retrieval of only a single parameter, from simulated (i.e., synthetic) data (as opposed to real data that is affected by noise and other uncontrollable errors), via an extremely-simple retrieval model.

Our inverse problem (in some respects similar to the ones treated in [3, 13]) concerns the retrieval of the material constant constituted by the real part of the shear wavespeed c_0 of a hard rock-like underground probed by a natural or man-made seismic disturbance (impulsive body wave) radiated by sources rather far underneath the ground. The data is furnished by the *total* shear-horizontal body wave response registered either at one, or several, point-like sensors located beneath or on

the ground.

1.1 Physical configuration and governing equations

The scattering configuration is a half space (termed: underground) bounded by a planar, stress-free surface (termed: ground). The half-space is infinite in the x and z directions of the $Oxyz$ cartesian coordinate system. Its intersection with the xOy plane defines (see fig.1):
i) the boundary $\Gamma_1 = \{y = y_1 = \text{const.} \ ; \ \forall x \in \mathbb{R}\}$, and
ii) the half-plane region $\Omega_0 = \{y < y_1 \ ; \ \forall x \in \mathbb{R}\}$, which is unbounded in the x-direction and of half-infinite extent in the y-direction,

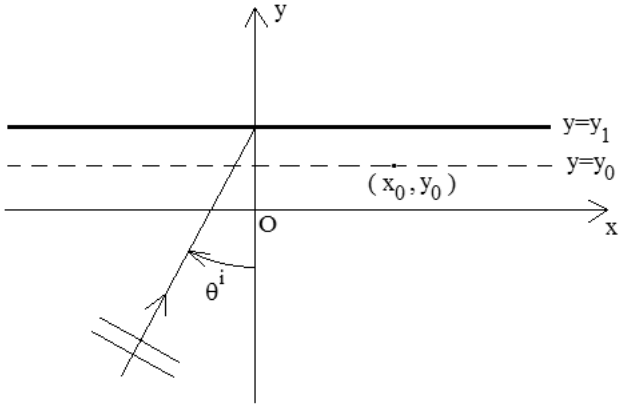

Figure 1: Problem configuration in the xOy plane. Γ is denoted by the dark line.

It is assumed that Ω_0 is filled with a linear, homogeneous, isotropic, possibly lossy, time-invariant (underground) medium M_0. The latter is characterized by the generally-complex, scalar, material constant c_0 related to the (generally-complex) rigidity μ_0 and density ρ_0 by $c_0 = \sqrt{\frac{\mu_0}{\rho_0}}$.

The underground is probed by a shear-horizontal elastodynamic wave emitted by a cylindrical source (with generator parallel to the z axis) far beneath the ground, so that the wave takes the form of a SH plane wave (only the z-component of the displacement associated with this wave is non-nil) in the vicinity of the stress-free (SF) boundary.

The SF nature of the boundary as well as the polarization of the incoming wave are responsible for the fact that the scattered displacement field is also SH-polarized (i.e., only its z-component is non-nil) and independent of z. Consequently, the problem is two-dimensional and is henceforth analyzed in the $x - y$ (sagittal) plane. Moreover the SF character of the boundary makes it impossible for the incident wave to penetrate into the half-space above the boundary, so that only the field below this boundary is of concern hereafter.

Let $\mathfrak{u}_0(\mathbf{x}, t)$ (with t the time and $\mathbf{x}$ the vector joining the origin O to the point (x, y)) be the z-component of the total field in Ω_0. This field is the sum of the incident field $\mathfrak{u}_0^+(\mathbf{x}, t)$ and (z-component of the) scattered field $\mathfrak{u}_0^-(\mathbf{x}, t)$:

$$\mathfrak{u}_0(\mathbf{x}, t) = \mathfrak{u}_0^+(\mathbf{x}, t) + \mathfrak{u}_0^-(\mathbf{x}, t) \ . \tag{1}$$

We express $\mathfrak{u}_0$ by the Fourier transform (in which ω is the angular frequency)

$$\mathfrak{u}_0(\mathbf{x},t) = \int_{-\infty}^{\infty} u_0(\mathbf{x},\omega)\exp(-i\omega t)d\omega \ , \tag{2}$$

with similar expressions for $\mathfrak{u}_0^+$ and $\mathfrak{u}_0^-$ so that the essential task (in both the forward and inverse scattering contexts) is to determine $u_0(\mathbf{x},\omega)$ constituting the response, at a sensor situated at $\mathbf{x}$, to the solicitation constituted by $u^+(\mathbf{x},\omega)$, the latter (an incoming wave with respect to O) being expressed by

$$u_0^+(\mathbf{x},\omega) = s(\omega)v^+(\mathbf{x},\omega) \ , \tag{3}$$

wherein

$$v^{\pm}(\mathbf{x},\omega) = \exp[i\omega\xi^{\pm}(\mathbf{x})] \ \ , \ \ \xi^{\pm}(\mathbf{x}) = \frac{x\sin\theta^i \pm (y-y_1)\cos\theta^i}{c_0} \ , \tag{4}$$

with $s(\omega)$ the spectrum of the excitation pulse such that $s(-\omega) = s^*(\omega)$ ($*$ designating the complex conjugate), $c_0' = \Re c_0 \geq 0$, $c_0'' = \Im c_0 \leq 0$, and $|\theta^i| < \frac{\pi}{2}$ so that $\cos\theta^i > 0$, with θ^i the incident angle.

The governing equations are:

$$\left(\Delta + \frac{\omega^2}{c_0^2}\right) u_0^{\pm}(\mathbf{x},\omega) = 0 \ ; \ \mathbf{x}\in\Omega_0 \ , \tag{5}$$

$$u_0^-(\mathbf{x},\omega) = u_0(\mathbf{x},\omega) - u_0^+(\mathbf{x},\omega) \sim \text{wave that is outgoing from O} \ ; \ \|\mathbf{x}\| \to \infty, \ , \ \mathbf{x}\in\Omega_0 \ , \tag{6}$$

$$\mu_0\partial_y u_0(\mathbf{x},\omega) = 0 \ ; \ \mathbf{x}\in\Gamma \ , \tag{7}$$

the last relation being the translation of the fact that the boundary is stress-free.

2 Solution of the forward problem in the space-frequency domain

It is easy to show that the solution of the boundary-value problem expressed by (1)-(7) is

$$u_0^-(\mathbf{x},\omega) = s(\omega)v^-(\mathbf{x},\omega) \ , \tag{8}$$

so that the total field is

$$u_0(\mathbf{x},\omega) = s(\omega)v^+(\mathbf{x},\omega) + s(\omega)v^-(\mathbf{x},\omega) \ . \tag{9}$$

3 Solution of the forward problem in the space-time domain

The sought-for solution is

$$\mathfrak{u}_0(\mathbf{x},t) = \int_{-\infty}^{\infty} s(\omega)[\exp(i\omega\xi^+(\mathbf{x})) + \exp(i\omega\xi^-(\mathbf{x}))]\exp(-i\omega t)d\omega \ , \tag{10}$$

3.1 Case of a flat excitation spectrum for all ω

We first treat the (ideal) case in which c_0 is real and

$$s(\omega) = \iota \exp(i\psi\omega) \ ; \ \forall \omega \in \mathbb{R} \ , \tag{11}$$

wherein ι and ψ are real constants with respect to ω. It ensues that

$$\mathfrak{u}_0^{\pm}(\mathbf{x},t) = \iota \int_{-\infty}^{\infty} \exp\left[i\omega\left(\xi^{\pm}(\mathbf{x}) + \psi - t\right)\right] d\omega = 2\pi\iota\delta\left(t - \psi - \xi^{\pm}(\mathbf{x})\right) \ , \tag{12}$$

with $\delta(\ )$ the Dirac delta distribution. The total space-time field at point (x,y) is then

$$\mathfrak{u}_0(\mathbf{x},t) = 2\pi\iota\delta\left(t - \psi - \xi^{+}(\mathbf{x})\right) + 2\pi\iota\delta\left(t - \psi - \xi^{-}(\mathbf{x})\right) \ , \tag{13}$$

which represents two spike-like pulses occurring at $t = t^+ = \psi + \xi^+$ and $t = t^- = \psi + \xi^-$.

We find

$$t^- - t^+ = -\frac{2(y - y_1)\cos\theta^i}{c_0} \geq 0 \ , \tag{14}$$

for $y \leq y_1$, which shows that the pulse associated with the scattered wave arrives later (or at the same time) as the pulse associated with the incident wave at the point $(x, y \leq y_1)$.

3.2 Case of a flat band-limited (i.e., rectangular) excitation spectrum

We now treat the less-idealized case in which c_0 is real and

$$s(\omega) = \begin{cases} \iota \exp(i\psi) & ; \ \forall \omega \in [\alpha,\beta] \\ 0 & ; \ \forall \omega \notin [\alpha,\beta] \end{cases} \ , \tag{15}$$

wherein ι and ψ are again real constants with respect to ω. It ensues that

$$\mathfrak{u}_0^{\pm}(\mathbf{x},t) = \iota \int_{\alpha}^{\beta} s(\omega) \exp\left[i\omega\left(\xi^{\pm}(\mathbf{x}) + \psi - t\right)\right] d\omega = \\ \iota(\beta - \alpha)\cos\left[\left(\frac{\beta+\alpha}{2}\right)\left(t - \psi - \xi^{\pm}(\mathbf{x})\right)\right] \mathrm{sinc}\left[\left(\frac{\beta-\alpha}{2}\right)\left(t - \psi - \xi^{\pm}(\mathbf{x})\right)\right] \ , \tag{16}$$

wherein $\mathrm{sinc}(x) = \frac{\sin x}{x}$.

The total space-time field at point (x,y) is then

$$\mathfrak{u}_0(\mathbf{x},t) = \iota(\beta - \alpha)\cos\left[\left(\frac{\beta+\alpha}{2}\right)\left(t - \psi - \xi^{+}(\mathbf{x})\right)\right] \mathrm{sinc}\left[\left(\frac{\beta-\alpha}{2}\right)\left(t - \psi - \xi^{+}(\mathbf{x})\right)\right] + \\ \iota(\beta - \alpha)\cos\left[\left(\frac{\beta+\alpha}{2}\right)\left(t - \psi - \xi^{-}(\mathbf{x})\right)\right] \mathrm{sinc}\left[\left(\frac{\beta-\alpha}{2}\right)\left(t - \psi - \xi^{-}(\mathbf{x})\right)\right] \ , \tag{17}$$

which represents two more or less-wide pulses whose amplitudes are extremal at $t = t^+ = \psi + \xi^+$ and $t = t^- = \psi + \xi^-$. As previously, the pulse associated with the scattered wave arrives later (or at the same time) as the pulse associated with the incident wave at the point $(x, y \leq y_1)$.

4 Travel-time inversion (TTI) for the retrieval of c_0 from the signal recorded at a single sensor

Again, we assume c_0 is real. We saw, in the previous two sections, that the signal recorded at a single sensor located at (x_0, y_0) consists of two pulses whose extrema are located at t^+ and t^- given by

$$t^{\pm} = \frac{x_0 \sin\theta^i \pm (y_0 - y_1)\cos\theta^i}{c_0} \ , \tag{18}$$

We assume that this signal (an amplitude versus time recording) is actually measured, and from this signal we are able to accurately pinpoint the instants t^+ and t^- at which the signal is extremal. Furthermore, we assume that the depth y_0 of the sensor is accurately known as is the angle of incidence θ^i. On the contrary, we have no knowledge of either x_0, ι and ψ, but, as we shall see, this is of no consequence. Therefore, the data for the TTI is t^+ and t^-, supplemented by the supposedly-known parameters y_0, and θ^i.

As before, we find (14) from which it follows that $c_0 = \frac{2(y_1-y_0)\cos\theta^i}{t^- - t^+}$ which shows that putting the sensor on the stress-free surface leads to trouble in this TTI scheme. An acceptable alternative is to bury the sensor at $y_0 = y_1 - \varepsilon$, with $\varepsilon > 0$ a supposedly-known quantity, whence $c_0 = \frac{2\varepsilon\cos\theta^i}{t^- - t^+}$. This is (an admittedly-primitive, due to the simplicity of the assumed geophysical configuration) TTI result for the retrieval of c_0, but has the virtue of showing that the accuracy of the retrieval of c_0 depends very much on the error of the data $t^- - t^+$ and somewhat on the error of y_0 (or ε) and θ^i.

5 Relation of the SPRCFI and SIRCFI cost functions

The drawbacks of (linear) TTI, in connection with the retrieval of the geometrical and mechanical parameters of more-typical geophysical configurations, are well-documented [16, 1]: inadequacy of models such as multilayers with plane-parallel interfaces, travel-time picking errors due amongst other factors to wave dispersion, the fact that arrivals with the lowest signal-to-noise ratio are not picked, etc. This (among other reasons) has led to the development of (nonlinear), frequency-domain [17, 16, 12, 3, 19, 14, 22] and time-domain [20, 21, 22, 8, 13] (so-called) full-waveform inversion (FWI) techniques [22]. The advantages and drawbacks of the two techniques are compared in [5]. A refreshing critique of FWI is given in [23].

Recall that, in the present investigation, the data is not actually measured, but rather simulated. This requires a *data simulation model* which we choose to be *mathematically* identical to the parameter retrieval model.

Let $\mathbf{p}$ be the set of true parameters involved in the data simulation model. The set $\mathbf{p}$, like its counterpart $\mathbf{P}$ of the retrieval model, is composed of two subsets: $\mathbf{r}$ comprising the to-be-retrieved parameters and $\mathbf{q}$ the remaining parameters. $\mathbf{p}$ is implicit in real (measured) data and explicit in (i.e., required to generate) simulated data. This means that the cost functional, employed to retrieve $\mathbf{R} \subset \mathbf{P}$, is blind to $\mathbf{r} \subset \mathbf{p}$ and $\mathbf{q}$, since it only sees the response data (be it measured or simulated).

The present study is mostly concerned with the case in which $\mathbf{r} = \{r_1\}$, and r_1 is the real part of the phase velocity of shear waves in the underground. Moreover, the set $\mathbf{Q}$ of the retrieval model (analogous to the set $\mathbf{q}$ of the data simulation model) is composed of the parameters (called

priors or nuisance parameters) that are fixed during the inversion and considered to be known, although with some *uncertainty*, for one or all of them. This uncertainty accounts for the fact that, in general, we are not committing the *inverse crime* (a situation that arises when all the priors in the retrieval model are identical to their counterparts in the data-simulation model and the two models are mathematically-identical) even though we are employing a parameter retrieval model that is mathematically-identical to the data simulation model [25].

Let the (measured or simulated) *space-frequency* data be $u(\mathbf{r}, \mathbf{q}, \omega)$ for ω in some interval (to be consistent with the term FWI, this frequency interval should be infinite). The limits of this interval, as well as the coordinates of the sensor(s) are parameters, amongst others, of the set $\mathbf{q}$. The corresponding parameter retrieval model involves $U(\mathbf{R}, \mathbf{Q}, \omega)$ for ω in some interval, and sensor locations, that are usually different (due to the previously-mentioned uncertainty) from those of the true data.

Let the (true) *space-time* data be $\mathfrak{u}(\mathbf{r}, \mathbf{q}, t)$ for t in some interval (to be consistent with the term FWI, this temporal interval should be infinite). The limits of this interval, as well as the coordinates of the sensor(s) are parameters, amongst others, of the set $\mathbf{q}$. The corresponding parameter retrieval model involves $\mathfrak{U}(\mathbf{R}, \mathbf{Q}, t)$ for t in some interval, and sensor locations, that are usually different (due to the previously-mentioned uncertainty) from those of the true data.

The SIRCFI cost functional is

$$C(\mathbf{R}, \mathbf{Q}) = \int_{-\infty}^{\infty} \|\mathfrak{U}(\mathbf{R}, \mathbf{Q}, t) - \mathfrak{u}(\mathbf{r}, \mathbf{q}, t)\|^2 dt \ , \tag{19}$$

and the aim is to obtain, by minimization of C, a set of values $\tilde{\mathbf{R}}$ which is as close as possible to the true set $\mathbf{r}$. Note that, owing to the fact that the space-time fields are real, the $\| \ \|$ sign can be replaced by $(\ )$.

The SPRCFI cost functional is

$$K(\mathbf{R}, \mathbf{Q}) = \int_{-\infty}^{\infty} \|U(\mathbf{R}, \mathbf{Q}, \omega) - u(\mathbf{r}, \mathbf{q}, \omega)\|^2 d\omega \ , \tag{20}$$

and the aim is to obtain, by minimization of K, a set of values $\tilde{\mathbf{R}}$ which is as close as possible to the true set $\mathbf{r}$. Note that U and u are complex functions of ω.

The question is: how does (19) relate to (20)? Recall that the signals $\mathfrak{U}$, $\mathfrak{u}$ are related to their spectra U, u respectively via the Fourier transforms

$$\mathfrak{U}(\mathbf{R}, \mathbf{Q}, t) = \int_{-\infty}^{\infty} U(\mathbf{R}, \mathbf{Q}, \omega) \exp(-i\omega t) d\omega \quad , \quad \mathfrak{u}(\mathbf{r}, \mathbf{q}, t) = \int_{-\infty}^{\infty} u(\mathbf{r}, \mathbf{q}, \omega) \exp(-i\omega t) d\omega \ . \tag{21}$$

After inserting (21) into (19), changing the orders of integration, making use of

$$\int_{-\infty}^{\infty} dt \ e^{-i(\omega - \omega')t} = 2\pi\delta(\omega - \omega') \ , \tag{22}$$

and of the sifting property of the Dirac distribution, we obtain

$$C(\mathbf{R}, \mathbf{Q}) = 2\pi K(\mathbf{R}, \mathbf{Q}) \ , \tag{23}$$

which is an expression of Parseval's theorem [12, 22].

It follows immediately that if the cost functional C exhibits deep minima, then K will exhibit the same amount and locations of deep minima. Thus, least squares cost functions involving response spectra give the same inversion result as least squares cost functions involving response signals.

This authorizes us to replace the SIRCFI method by the SPRCFI method to solve the inverse problem (via the cost functional K). The enormous advantage of doing so makes itself felt in the case in which the data is a (space-time) signal (as is usual) and the retrieval model is of the space-frequency variety [17, 16, 3, 19, 14, 22]. In this case, we must make a single (for the single sets $\mathbf{r}, \mathbf{q}$) Fourier transform to obtain the spectrum of the true data in the SPRCFI method, whereas in the SIRCFI method we would have to make many Fourier transforms of $U(\mathbf{R}, \mathbf{Q}, \omega)$ for the set $\mathbf{R}$ that is varied during the construction of the cost function.

6 Theoretical aspects of the SPRCFI method for single sensor data

6.1 Definition of the SPRCFI cost functional for single sensor data

We now assume that the data is registered at a single point-like sensor located at (x_0, y_0) beneath or on the ground and adopt the shorthand notation: $K = K(\mathbf{R}, \mathbf{Q})$, $U(\omega) = U_0(\mathbf{R}, \mathbf{Q}, \omega)$, $u(\omega) = u_0(\mathbf{r}, \mathbf{q}, \omega)$, $v^{\pm}(\omega) = v^{\pm}(x_0, y_0, \omega) = \exp(i\omega\xi^{\pm})$, $\xi^{\pm} = \xi^{\pm}(x_0, y_0)$. We saw that

$$u(\omega) = s(\omega)v(\omega) = s(\omega)v^{+}(\omega) + s(\omega)v^{-}(\omega) \ , \tag{24}$$

so that, employing a similar retrieval model, we have

$$U(\omega) = S(\omega)V(\omega) = S(\omega)V^{+}(\omega) + S(\omega)V^{-}(\omega) \ , \tag{25}$$

wherein (again for the homogeneous underground bounded by the stress-free ground at $y = Y_1$ solicited by a plane wave)

$$V^{\pm}(\omega) = \exp(i\omega\Xi^{\pm}) \ \ , \ \ \Xi^{\pm} = \frac{X_0 \sin\Theta^i \pm (Y_0 - Y_1)\cos\Theta^i}{C_0} \ . \tag{26}$$

The normalized SPRCFI cost functional for single sensor data is

$$\kappa = \frac{\int_{-\infty}^{\infty} \|u(\omega) - U(\omega)\|^2 d\omega}{\int_{-\infty}^{\infty} \|u(\omega)\|^2 d\omega} \ . \tag{27}$$

6.2 The case of a rectangular excitation spectrum

If the spectrum $s(\omega)$ of u is assumed to be of finite bandwidth $[\alpha, \beta]$, it is reasonable to assume that the spectrum $S(\omega)$ of U is also of finite (but not necessarily the same) bandwidth $[\mathcal{A}, \mathcal{B}]$, so that the integrals in the previous expression are necessarily over the finite bandwidth $[\omega_b, \omega_e]$, the issue of the relation of ω_b to α, $\mathcal{A}$ and of ω_e to β, $\mathcal{B}$ being considered further on. Consequently,

$$\kappa = \frac{\int_{\omega_b}^{\omega_e} \|u(\omega) - U(\omega)\|^2 d\omega}{\int_{\omega_b}^{\omega_e} \|u(\omega)\|^2 d\omega} = \frac{K}{K_1} \ . \tag{28}$$

Owing to (24)-(25), we obtain

$$K = \int_{\omega_b}^{\omega_e} \|s(\omega)v(\omega) - S(\omega)V(\omega)\|^2 d\omega = K_1 + K_2 + K_3 + K_4 + K_5 + K_6 \ . \tag{29}$$

wherein (with $\|s(\omega)\|^2 = \|\iota \exp(i\psi\omega)\|^2 = \iota^2$, $\|S(\omega)\|^2 = \|\mathcal{I} \exp(i\Psi\omega)\|^2 = \mathcal{I}^2$, $s(\omega)S^*(\omega) = \iota\mathcal{I}e^{i(\psi-\Psi)}$):

$$K_1 = \iota^2 \int_{\omega_b}^{\omega_e} \left[\|v^+(\omega)\|^2 + 2\Re\left(v^+(\omega)v^{-*}(\omega)\right) + \|v^-(\omega)\|^2\right] d\omega \ , \tag{30}$$

$$K_2 = -2\iota\mathcal{I}\Re\left(e^{i(\psi-\Psi)} \int_{\omega_b}^{\omega_e} v^+(\omega)V^{+*}(\omega)d\omega\right) \quad , \quad K_3 = -2\iota\mathcal{I}\Re\left(e^{i(\psi-\Psi)} \int_{\omega_b}^{\omega_e} v^+(\omega)V^{-*}(\omega)d\omega\right) \ , \tag{31}$$

$$K_4 = -2\iota\mathcal{I}\Re\left(e^{i(\psi-\Psi)} \int_{\omega_b}^{\omega_e} v^-(\omega)V^{+*}(\omega)d\omega\right) \ , \quad K_5 = -2\Re\left(\iota\mathcal{I}e^{i(\psi-\Psi)} \int_{\omega_b}^{\omega_e} v^-(\omega)V^{-*}(\omega)d\omega\right) \ , \tag{32}$$

$$K_6 = \mathcal{I}^2 \int_{\omega_b}^{\omega_e} \left[\|V^+(\omega)\|^2 + 2\Re\left(V^+(\omega)V^{-*}(\omega)\right) + \|V^-(\omega)\|^2\right] d\omega \ . \tag{33}$$

We can write

$$K_1 = K_{11} + K_{12} + K_{13} \ , \tag{34}$$

wherein, since there is no ambiguity as to the fact that in K_1, $[\omega_b, \omega_e] = [\alpha, \beta]$:

$$K_{11} = \iota^2 \int_{\alpha}^{\beta} \|v^+(\omega)\|^2 d\omega \quad , \quad K_{12} = 2\iota^2\Re \int_{\alpha}^{\beta} v^+(\omega)v^{-*}(\omega)d\omega \quad , \quad K_{13} = \iota^2 \int_{\alpha}^{\beta} \|v^-(\omega)\|^2 d\omega \ . \tag{35}$$

6.3 Cost functional relative to the homogeneous underground bounded by a stress-free ground problem

Recalling the definitions of $v^{\pm}(\omega)$ and $V^{\pm}(\omega)$, enables us to find, via (16):

$$\begin{aligned} K_{11} &= \iota^2(\beta-\alpha)\cos\left[\left(\frac{\beta+\alpha}{2}\right)(\xi^+ - \xi^{+*})\right] \mathrm{sinc}\left[\left(\frac{\beta-\alpha}{2}\right)(\xi^+ - \xi^{+*})\right] \quad , \\ K_{12} &= 2\iota^2(\beta-\alpha)\cos\left[\left(\frac{\beta+\alpha}{2}\right)(\xi^+ - \xi^{-*})\right] \mathrm{sinc}\left[\left(\frac{\beta-\alpha}{2}\right)(\xi^+ - \xi^{-*})\right] \quad , \\ K_{13} &= \iota^2(\beta-\alpha)\cos\left[\left(\frac{\beta+\alpha}{2}\right)(\xi^- - \xi^{-*})\right] \mathrm{sinc}\left[\left(\frac{\beta-\alpha}{2}\right)(\xi^- - \xi^{-*})\right] \quad . \end{aligned} \tag{36}$$

We can also write

$$K_6 = K_{61} + K_{62} + K_{63} \ , \tag{37}$$

wherein, due to there being no ambiguity as to the fact that in K_6, $[\omega_b, \omega_e] = [\mathcal{A}, \mathcal{B}]$:

$$K_{61} = \mathcal{I}^2 \int_{\mathcal{A}}^{\mathcal{B}} \|V^+(\omega)\|^2 d\omega \quad , \quad K_{62} = 2\mathcal{I}^2\Re \int_{\mathcal{A}}^{\mathcal{B}} V^+(\omega)V^{-*}(\omega)d\omega \quad , \quad K_{13} = \mathcal{I}^2 \int_{\mathcal{A}}^{\mathcal{B}} \|V^-(\omega)\|^2 d\omega \ , \tag{38}$$

so that by proceeding as previously, we find

$$K_{61} = \mathcal{I}^2(\mathcal{B}-\mathcal{A})\cos\left[\left(\frac{\mathcal{B}+\mathcal{A}}{2}\right)(\Xi^+ - \Xi^{+*})\right]\mathrm{sinc}\left[\left(\frac{\mathcal{B}-\mathcal{A}}{2}\right)(\Xi^+ - \Xi^{+*})\right] \quad ,$$
$$K_{62} = 2\mathcal{I}^2(\mathcal{B}-\mathcal{A})\cos\left[\left(\frac{\mathcal{B}+\mathcal{A}}{2}\right)(\Xi^+ - \Xi^{-*})\right]\mathrm{sinc}\left[\left(\frac{\mathcal{B}-\mathcal{A}}{2}\right)(\Xi^+ - \Xi^{-*})\right] \quad ,$$
$$K_{63} = \mathcal{I}^2(\mathcal{B}-\mathcal{A})\cos\left[\left(\frac{\mathcal{B}+\mathcal{A}}{2}\right)(\Xi^- - \Xi^{-*})\right]\mathrm{sinc}\left[\left(\frac{\mathcal{B}-\mathcal{A}}{2}\right)(\Xi^- - \Xi^{-*})\right] \quad . \quad (39)$$

We now turn to the terms involving the product of $u_0^+ = sv^+$ and $U_0^{-*} = S^*V^{-*}$ or $u_0^{+*} = s^*v^{+*}$ and $U_0^- = SV^-$, the question being how to relate ω_b to α, $\mathcal{A}$ and ω_e to β, $\mathcal{B}$. Recall that $\beta > \alpha$ and $\mathcal{B} > \mathcal{A}$. We assume, as is reasonable, that $\mathcal{B} > \alpha$ and $\mathcal{A} < \beta$. Then, only four situations are possible: 1) $\mathcal{A} \geq \alpha$ and $\mathcal{B} \leq \alpha$, 2) $\mathcal{A} \geq \alpha$ and $\mathcal{B} \geq \alpha$, 3) $\mathcal{A} \leq \alpha$ and $\mathcal{B} \leq \alpha$, 4) $\mathcal{A} \leq \alpha$ and $\mathcal{B} \geq \alpha$. In the first situation, $S = s = 0$ for $\omega < \mathcal{A}$ and $S = s = 0$ for $\omega > \mathcal{B}$ so that the only interval in which the product sS^* is non-zero is $[\mathcal{A}, \mathcal{B}]$, whence $\omega_b = \mathcal{A}$ and $\omega_e = \mathcal{B}$. In the second situation, $S = s = 0$ for $\omega < \mathcal{A}$ and $S = s = 0$ for $\omega > \beta$ so that the only interval in which the product sS^* is non-zero is $[\mathcal{A}, \beta]$, whence $\omega_b = \mathcal{A}$ and $\omega_e = \beta$. In the third situation, $S = s = 0$ for $\omega < \alpha$ and $S = s = 0$ for $\omega > \mathcal{B}$ so that the only interval in which the product sS^* is non-zero is $[\alpha, \mathcal{B}]$, whence $\omega_b = \alpha$ and $\omega_e = \mathcal{B}$. In the fourth situation, $S = s = 0$ for $\omega < \alpha$ and $S = s = 0$ for $\omega > \beta$ so that the only interval in which the product sS^* is non-zero is $[\alpha, \beta]$, whence $\omega_b = \alpha$ and $\omega_e = \beta$.

With this in mind, we find:

$$K_2 = -2\iota\mathcal{I}\Re\left(e^{i(\psi-\Psi)}\int_{\omega_b}^{\omega_e} e^{i\omega(\xi^+ - \Xi^{+*})}d\omega\right) \quad , \quad K_3 = -2\iota\mathcal{I}\Re\left(e^{i(\psi-\Psi)}\int_{\omega_b}^{\omega_e} e^{i\omega(\xi^+ - \Xi^{-*})}d\omega\right) \quad ,$$
$$K_4 = -2\iota\mathcal{I}\Re\left(e^{i(\psi-\Psi)}\int_{\omega_b}^{\omega_e} e^{i\omega(\xi^- - \Xi^{+*})}d\omega\right) \quad , \quad K_5 = -2\Re\iota\mathcal{I}\left(e^{i(\psi-\Psi)}\int_{\omega_b}^{\omega_e} e^{i\omega(\xi^- - \Xi^{-*})}d\omega\right) \quad , \quad (40)$$

and again make use of (16) to obtain

$$K_2 = -2\iota\mathcal{I}(\omega_e-\omega_b)\Re\left(e^{i(\psi-\Psi)}\cos\left[\left(\frac{\omega_e+\omega_b}{2}\right)(\xi^+ - \Xi^{+*})\right]\mathrm{sinc}\left[\left(\frac{\omega_e-\omega_b}{2}\right)(\xi^+ - \Xi^{+*})\right]\right) \quad ,$$
$$K_3 = -2\iota\mathcal{I}(\omega_e-\omega_b)\Re\left(e^{i(\psi-\Psi)}\cos\left[\left(\frac{\omega_e+\omega_b}{2}\right)(\xi^+ - \Xi^{-*})\right]\mathrm{sinc}\left[\left(\frac{\omega_e-\omega_b}{2}\right)(\xi^+ - \Xi^{-*})\right]\right) \quad ,$$
$$K_4 = -2\iota\mathcal{I}(\omega_e-\omega_b)\Re\left(e^{i(\psi-\Psi)}\cos\left[\left(\frac{\omega_e+\omega_b}{2}\right)(\xi^- - \Xi^{+*})\right]\mathrm{sinc}\left[\left(\frac{\omega_e-\omega_b}{2}\right)(\xi^- - \Xi^{+*})\right]\right) \quad ,$$
$$K_5 = -2\iota\mathcal{I}(\omega_e-\omega_b)\Re\left(e^{i(\psi-\Psi)}\cos\left[\left(\frac{\omega_e+\omega_b}{2}\right)(\xi^- - \Xi^{-*})\right]\mathrm{sinc}\left[\left(\frac{\omega_e-\omega_b}{2}\right)(\xi^- - \Xi^{-*})\right]\right) \quad . \quad (41)$$

6.4 Properties of the sinc function

Consider the function

$$\sigma(\chi) = \mathrm{sinc}(k^-\chi) = \frac{\sin(k^-\chi)}{k^-\chi} \quad , \quad (42)$$

wherein $k^- = \frac{\varpi^-}{c}$ and χ are supposed to be real and ϖ^- is one-half of a bandwidth (in our problem). This function:

1- is oscillatory, but its envelope decays as $(k^-\chi)^{-1}$,
2- attains its maximal positive value = 1 at $k^-\chi = 0$,
3- attains its maximal negative value $\sigma(k^-\chi) = -(\frac{3\pi}{2})^{-1}$ at $k^-\chi = \pm\frac{3\pi}{2}$, i.e., at $\chi = \pm\frac{3\pi}{2k^-}$.

Consequently, $\sigma(\chi)$ is of the form of a (so-called main) pulse for $\chi \in [-\frac{3\pi}{2k^-}, \frac{3\pi}{2k^-}]$ and the width of this pulse is all the smaller, the larger is k^-. In other words, the sharpness of the main pulse (its height/width) increases with increasing k^-, or increasing ϖ^-, the latter being one half the bandwidth of the excitation spectrum.

6.5 Properties of the sinc cos product

Consider the function

$$\upsilon(\chi) = \mathrm{sinc}(k^-\chi)\cos(k^+\chi) \ , \tag{43}$$

wherein $k^+ = \frac{\varpi^+}{c}$ and ϖ^+ is the mean frequency of the excitation spectrum. The cos term, which modulates the sinc term, has maxima at $\chi = \frac{2n\pi}{k^+}$; $n \in \mathbb{Z}$, or, in other words, the frequency (in terms of χ) of the cos term increases with k^+. If account is not taken of this modulation, the main pulse associated with $\upsilon(\chi)$ becomes sharper with increasing k^- and/or k^+. Note that $\upsilon(0) = 1$.

An interesting situation arises when $k^- \approx 0$ which we call the case of *near-monochromaticity*; then sinc ≈ 1 which means that $\upsilon \approx \cos(k^+\chi)$ and the variation of this function (whose minima ≈ -1) is all the more rapid the larger is k^+. This unfavorable situation, which is synonymous with the occurrence of multiple deep minima in the cost function, can be avoided by increasing the bandwidth k^- of the excitation spectrum. The recognition of this fact is one of our principal contributions to the (re-) introduction of the SPRCFI method.

Another interesting situation arises when $k^+ \approx k^- = k$, which occurs for $\omega_e >> \omega_b$. Then $\upsilon \approx \mathrm{sinc}(2k\chi)$ which represents an unmodulated signal the main pulse of which is twice as wide as the previous modulated sinc function. Thus, by having the lower frequency of the excitation spectrum as small as possible compared to the upper frequency, one is able to eliminate the annoying modulation-induced secondary minima in the main pulse, but at the expense of reducing the sharpness of this pulse. We shall see further on that this is the situation of the excitation spectra of typical moderate-amplitude seismic signals.

6.6 Cost functional relative to the homogeneous, elastic underground bounded by a stress-free ground problem of the retrieval of C_0

The fact that the underground is elastic means that c_0 (the parameter we wish to retrieve) is real (i.e., $c_0 = c_0'$). Thus, we consider C_0 likewise to be real (i.e., $C_0 = C_0'$). This is assumed in all that follows and entails $\xi^{\pm *} = \xi^{\pm}$, $\Xi^{\pm *} = \Xi^{\pm}$. We define the new variables:

$$\gamma = \beta + \alpha \ , \ \ \eta = \beta - \alpha \ , \tag{44}$$

which can be recognized as twice the central frequency and bandwidth respectively of the excitation spectrum. The corresponding priors are $\mathcal{G} = \mathcal{B} + \mathcal{A}$ and $\mathcal{E} = \mathcal{B} - \mathcal{A}$, whence (on account of the

material in sects. 6.4 and 6.5)

$$K_1(c_0) = 2\iota^2\eta\left(1+\cos\left[\left(\frac{\gamma}{2}\right)(\xi^+-\xi^-)\right]\mathrm{sinc}\left[\left(\frac{\eta}{2}\right)(\xi^+-\xi^-)\right]\right)\ , \tag{45}$$

$$K_6(C_0) = 2\mathcal{I}^2\mathcal{E}\left(1+\cos\left[\left(\frac{\mathcal{G}}{2}\right)(\Xi^+-\Xi^-)\right]\mathrm{sinc}\left[\left(\frac{\mathcal{E}}{2}\right)(\Xi^+-\Xi^-)\right]\right)\ , \tag{46}$$

$$\begin{aligned}
K_2(C_0) &= -2\iota\mathcal{I}(\omega_e-\omega_b)\cos(\psi-\Psi)\cos\left[\left(\frac{\omega_e+\omega_b}{2}\right)(\xi^+-\Xi^+)\right]\mathrm{sinc}\left[\left(\frac{\omega_e-\omega_b}{2}\right)(\xi^+-\Xi^+)\right]\ ,\\
K_3(C_0) &= -2\iota\mathcal{I}(\omega_e-\omega_b)\cos(\psi-\Psi)\cos\left[\left(\frac{\omega_e+\omega_b}{2}\right)(\xi^+-\Xi^-)\right]\mathrm{sinc}\left[\left(\frac{\omega_e-\omega_b}{2}\right)(\xi^+-\Xi^-)\right]\ ,\\
K_4(C_0) &= -2\iota\mathcal{I}(\omega_e-\omega_b)\cos(\psi-\Psi)\cos\left[\left(\frac{\omega_e+\omega_b}{2}\right)(\xi^--\Xi^+)\right]\mathrm{sinc}\left[\left(\frac{\omega_e-\omega_b}{2}\right)(\xi^--\Xi^+)\right]\ ,\\
K_5(C_0) &= -2\iota\mathcal{I}(\omega_e-\omega_b)\cos(\psi-\Psi)\cos\left[\left(\frac{\omega_e+\omega_b}{2}\right)(\xi^--\Xi^-)\right]\mathrm{sinc}\left[\left(\frac{\omega_e-\omega_b}{2}\right)(\xi^--\Xi^-)\right]\ .
\end{aligned} \tag{47}$$

We observe that:

1- $K_1 > 0$ and $K_6 > 0$ for reasonably-small $|\xi^+ - \xi^-|$ and $|\Xi^+ - \Xi^-|$,
2- K_1 does not depend on C_0,
3- $K_2 < 0$, $K_3 < 0$, $K_4 < 0$ and $K_5 < 0$, if it assumed (as is reasonable) that ι and $\mathcal{I}$ have the same signs and Ψ is not too different from ψ, and for reasonably-small $|\xi^+ - \Xi^+|$, $|\xi^+ - \Xi^-|$, $|\xi^- - \Xi^+|$, $|\xi^- - \Xi^-|$.

This means that the establishment of a minimum in the global cost functional κ can only be the result of one or all of the $K_2,\ K_3,\ K_4,\ K_5$ attaining their minimum negative value$= -2\iota\mathcal{I}(\omega_e-\omega_b)$. This occurs, as concerns K_2, when $\xi^+ - \Xi^+ = 0$, or for

$$C_0 = C_0^{(2)} = c_0\left(\frac{X_0\sin\Theta^i + (Y_0-Y_1)\cos\Theta^i}{x_0\sin\theta^i + (y_0-y_1)\cos\theta^i}\right)\ . \tag{48}$$

It occurs, as concerns K_3, when $\xi^+ - \Xi^- = 0$, or for

$$C_0 = C_0^{(3)} = c_0\left(\frac{X_0\sin\Theta^i - (Y_0-Y_1)\cos\Theta^i}{x_0\sin\theta^i + (y_0-y_1)\cos\theta^i}\right)\ . \tag{49}$$

It occurs, as concerns K_4, when $\xi^- - \Xi^+ = 0$, or for

$$C_0 = C_0^{(4)} = c_0\left(\frac{X_0\sin\Theta^i + (Y_0-Y_1)\cos\Theta^i}{x_0\sin\theta^i - (y_0-y_1)\cos\theta^i}\right)\ . \tag{50}$$

It occurs, as concerns K_5, when $\xi^- - \Xi^- = 0$, or for

$$C_0 = C_0^{(5)} = c_0\left(\frac{X_0\sin\Theta^i - (Y_0-Y_1)\cos\Theta^i}{x_0\sin\theta^i - (y_0-y_1)\cos\theta^i}\right)\ . \tag{51}$$

These, and the previous, formulae enable us to predict several notable features of the cost function:

A- The single deepest minimum of the global cost functional should occur when all four $C_0^{(j)}$ are equal, and this happens when $y_0 = y_1$ and $Y_0 = Y_1$. Thus the deepest minimum occurs at $C_0^{(1)}$ when the true sensor is on the stress-free surface (i.e., $y_0 = y_1$) and the prior Y_1 is certain (i.e., $Y_1 = y_1$). This happens, regardless of the uncertainty of X_0 and Θ^i, but the accuracy of the retrieval of C_0 *does depend* on the uncertainty of X_0 and Θ^i.
B- When, however, the true sensor is below the free surface (i.e., $y_0 < y_1$), and X_0, Y_0, Y_1 and Θ^i are certain, two deep minima of the component cost functionals occur at the same location $C_0^{(2)} = C_0^{(5)} = c_0$, with the (possibly-observable) occurrence of two other deep minima not located at $C_0 = c_0$; this points to the possibility of the non-uniqueness of the parameter-retrieval problem even in an inverse crime situation.
C- When any one of the priors X_0, Y_0, Y_1 and Θ^i are uncertain, the gloabl cost functional may exhibit multiple deep minima, none of which are at $C_0 = c_0$ or the cost functional may exhibit a single deep minimum which is not at $C_0 = c_0$, this meaning that prior uncertainties generally have the effect of producing non-unique retrievals or retrievals that are inaccurate.
D- To the question of how the central frequency and bandwidth of the excitation spectrum affects the multiplicity of deep minima in the global cost functional, we refer the reader to the material in sect. 6.5
E- It proves to be advantageous to plot (and look for the location of the minimum of this functional) K versus $1/C_0$ rather than K versus C_0 due to the fact that arguments of the sinc cos functions in K depend on $1/C_0$ rather than on C_0 .
F- K_6 is a constant with respect to C_0 whenever the sensor is on the stress-free surface (because $Y_0 = Y_1 \Rightarrow \Xi^+ = \Xi^-$.
G- Although we are here studying one of the simplest seismic inverse problems, the number of involved, non-linearly-related, parameters is considerable: ten true parameters forming the set $\mathbf{p} = \{x_0, y_0, c_0', c_0'', y_1, \theta^i, \iota, \psi, \alpha, \beta\}$ and nine parameters forming the set $\mathbf{Q} = \{X_0, Y_0, C_0'', Y_1, \Theta^i, \mathcal{I}, \Psi, \mathcal{A}, \mathcal{B}\}$.
H- To further simplify the problem, we suppose henceforth that $C_0'' = c_0'' = 0$ and that there is no uncertainty on the priors Y_1 and Ψ.

7 Numerical results for the SPRCFI method employing data registered at one sensor on the ground in a realistic geophysical situation

The following results apply to a rectangular excitation spectrum and to the true parameter set: $x_0 = 100$ m, $y_0 = 100$ m, $c_0' = 3000$ m/s, $c_0'' = 0$ km/s, $y_1 = 100$ m, $\theta^i = 60°$, $\iota = 10^{-4}$ m, unless specified otherwise.

Each of the following figures is composed of six panels. Let $\kappa_j = \frac{K_j}{K_1}$. Then, the upper left, middle and right panels depict the component costs κ_2, κ_3, κ_4 respectively as a function of the slowness $1/C_0$ whereas the lower left, middle and right panels depict κ_5, κ_6 and the total cost κ respectively. The dashed vertical line in these panels indicates the target value $1/c_0$, with the understanding that $c_0 = c_0'$ and $C_0 = C_0'$. The boldfaced numbers in the captions indicate which numbers are changing from one figure to the next in a given set of figures.

7.1 The inverse crime situation

The parameters corresponding to this inverse crime situation are: $\delta_{x_0} = \frac{X_0 - x_0}{x_0} = 0$, $\delta_{y_0} = \frac{Y_0 - y_0}{y_0} = 0$, $\delta_{y_1} = \frac{Y_1 - y_1}{y_1} = 0$, $\delta_{\theta^i} = \frac{\Theta^i - \theta^i}{\theta^i} = 0$, $\delta_\iota = \frac{\mathcal{I} - \iota}{\iota} = 0$, $\delta_\psi = \frac{\Psi - \psi}{\psi} = 0$, $\delta_\gamma = \frac{G - \gamma}{\gamma} = 0$ and $\delta_\eta = \frac{E - \eta}{\eta} = 0$.

7.1.1 Variable γ

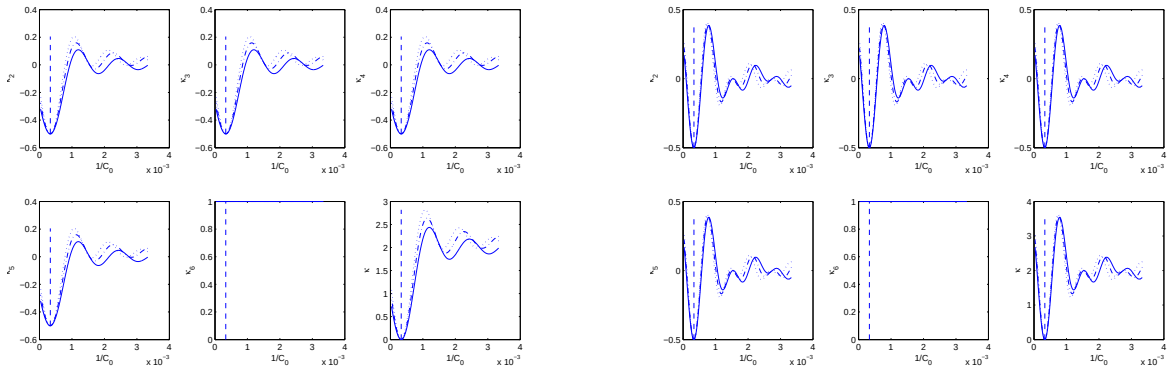

(a) (b)

Figure 2: (a): $\theta^i = 60°$, η=60 Hz, γ=**60.1** Hz (——), **70.1** Hz (-.-.-.-), **80.1** Hz (.....). The global minimum is at 2998 m/s for all three values of γ (3000 m/s for more samples along the $1/C_0$ axis. (b): $\theta^i = 60°$, η=60 Hz, γ=**150.1** Hz (——), **160.1** Hz (-.-.-.-), **170.1** Hz (.....). The global minimum is at 2998 m/s for all three values of γ.

In fig. 2, we observe, in agreement with the theoretical prediction in sect. 6.5, that increasing γ increases the amount of secondary minima. Since we are in the inverse crime situation, the retrievals (via the position of the global minimum) are nose-on to the target, and all the component cost functionals are identical except κ_6 which is constant with respect to $1/C_0$ due to property F in sect. 6.6. This feature is common to all the following results pertaining to a sensor located on the free surface.

7.1.2 Variable η

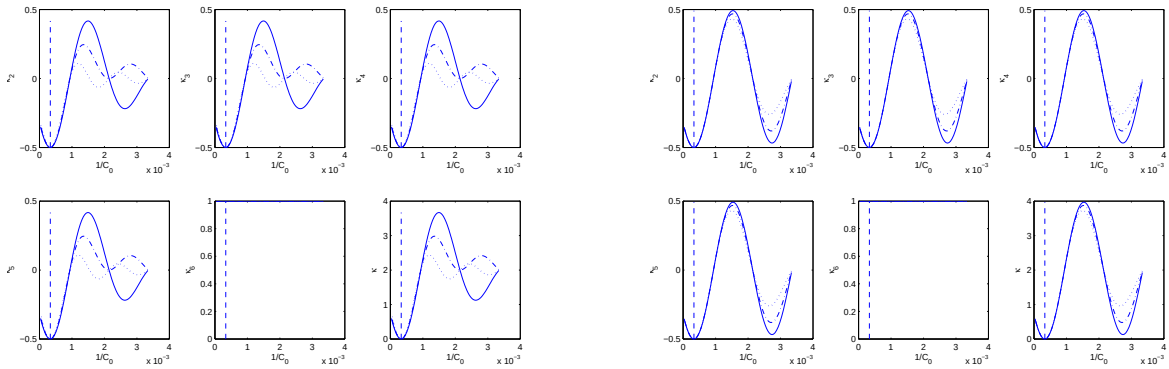

(a) (b)

Figure 3: (a): $\theta^i = 60°$, γ=60.1 Hz, η = **20** Hz (——), **40** Hz (-.-.-.-), **60** Hz (.....). The global minimum is at 2998 m/s for all three values of η.
(b): $\theta^i = 60°$. γ=60.1 Hz. η = **6** Hz (——), **12** Hz (-.-.-.-), **18** Hz (.....). The global minimum is at 2998 m/s for all three values of η.

In fig. 3, we observe, in agreement with the theoretical prediction in sect. 6.5, that decreasing η produces the effect of increasing the depth of the troughs of the secondary minima. For the smallest η, one is in the situation of near-monochromaticity whereby it becomes nearly-impossible to distinguish the global minimum from the secondary minima. This fact constitutes one of the principal findings of this investigation. It suggests the recommendation that to promote uniqueness of retrievals (i.e., to tend towards the situation of a single deep minimum), one should choose (if this is feasible) data obtained from probe radiation whose spectrum is as wide as possible.

7.1.3 Variable θ^i

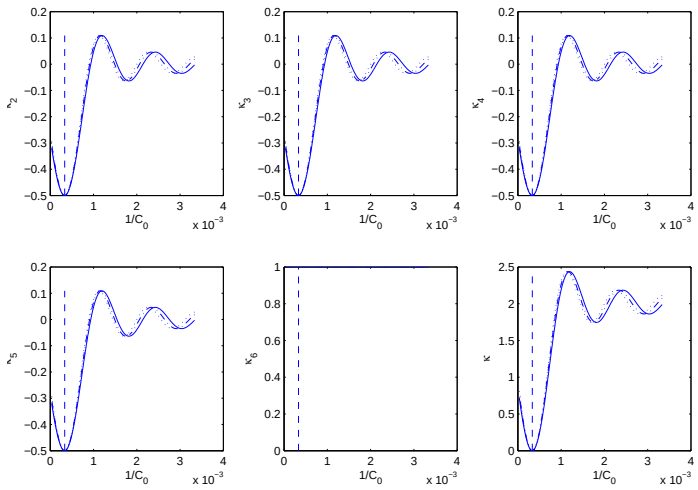

Figure 4: $\theta^i = \mathbf{6}0°$ (——), $\mathbf{70}°$ (-.-.-.-), $\mathbf{80}°$ (.....). γ=60.1 Hz. $\eta = 60$ Hz. The target (- - - -) is at 3000 m/s, whereas the global minimum is at 2998 m/s for all three values of θ^i.

Fig. 4 shows that the aspect of the component and total cost functions is relatively insensitive to θ^i, this being largely due to the facts that: we are in an inverse crime situation, the sensor is on the ground and both γ and η are small.

7.1.4 Variable x_0

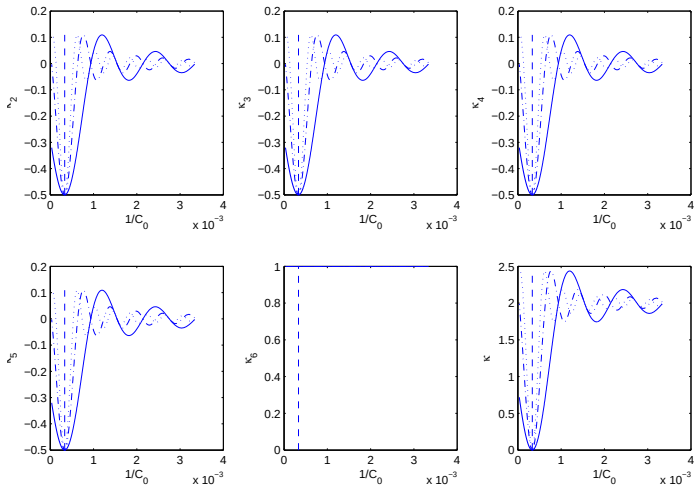

Figure 5: $x_0 = \mathbf{100}$ m (——), **200** m (-.-.-.-), **300** m (.....). $\theta^i = 60°$. γ=60.1 Hz. $\eta = 60$ Hz. The target (- - - -) is at 3000 m/s, whereas the global minimum is at 2998 m/s for all three values of x_0.

Fig. 5 shows that the increasing x_0 produces an effect (i.e., increasing the number of secondary minima) on the cost functions that is similar to that of increasing γ.

7.2 The (usual) situation in which one or more priors are uncertain

The parameters corresponding to this inverse crime situation are: $\delta_{x_0} \neq 0$ and/or $\delta_{y_0} \neq 0$ and/or $\delta_{\theta^i} \neq 0$ and/or $\delta_\iota \neq 0$ and/or $\delta_\gamma \neq 0$ and/or $\delta_\eta \neq 0$.

7.2.1 The only uncertain prior is Θ^i. Variable γ

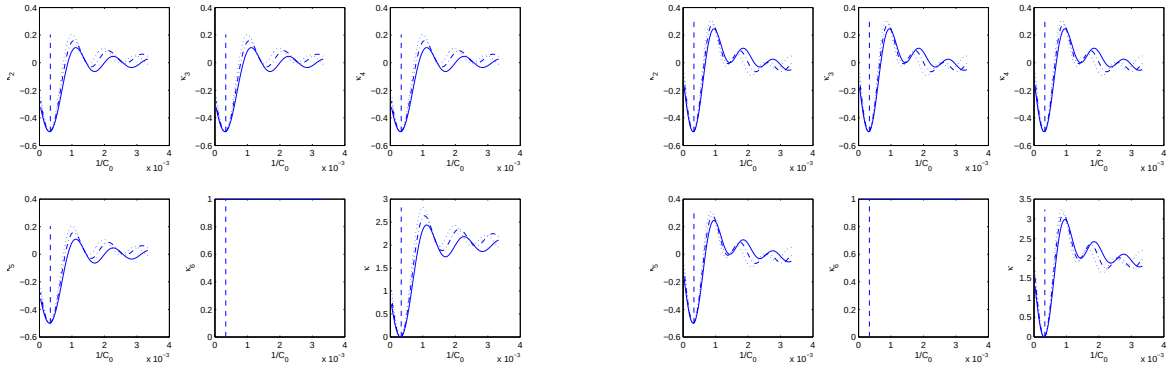

(a) (b)

Figure 6: (a): $\theta^i = 60°$, $\delta_{\theta^i} = 0.13333$, γ=**60.1** Hz (——), **70.1** Hz (-.-.-.-), **80.1** Hz (.....). η=60 Hz. The global minimum is at 3211 m/s for all three values of γ.
(b): $\theta^i = 60°$, $\delta_{\theta^i} = 0.13333$, γ=**90.1** Hz (——), **100.1** Hz (-.-.-.-), **110.1** Hz (.....). η=60 Hz. The global minimum is at 3211 m/s for all three values of γ.

In fig. 6 we see that, due to the relatively-small uncertainty in Θ^i, the overall behavior of the cost functions with respect to $1/C_0$ and changes of γ is similar to what was found in the inverse crime situation. However, the retrieval of the velocity is somewhat off-target (as manifested by a small shift of the position of the global minimum) due to the fact that $\Theta^i \neq \theta^i$.

7.2.2 The only uncertain prior is Θ^i. Variable η

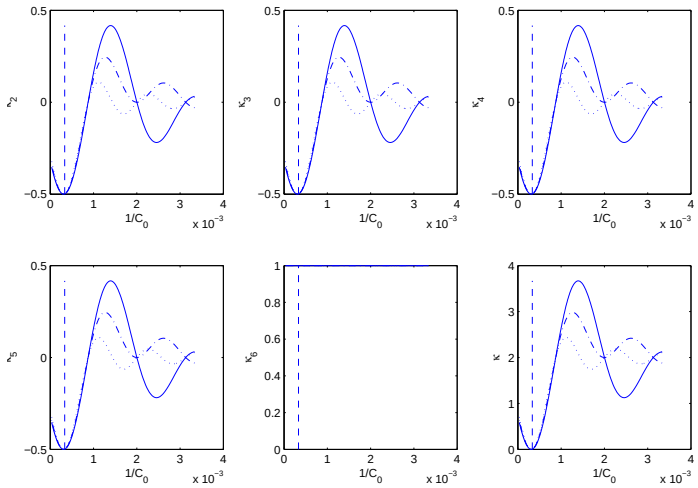

Figure 7: $\theta^i = 60°$. $\delta_{\theta^i} = 0.13333$. γ=60.1 Hz. η = **20** Hz (——), **40** Hz (-.-.-.-), **60** Hz (.....). The target (- - - -) is at 3000 m/s, whereas the global minimum is at 3211 m/s for all three values of γ.

The result, In fig. 7, together with the one in fig.6, show, in agreement with the theoretical prediction A of sect. 6.6, that the position of the global minimum is independent of γ and ν, but dependent on the discrepancy between Θ^i and θ^i.

7.2.3 The only uncertain prior is $\mathcal{G}$. Variable η

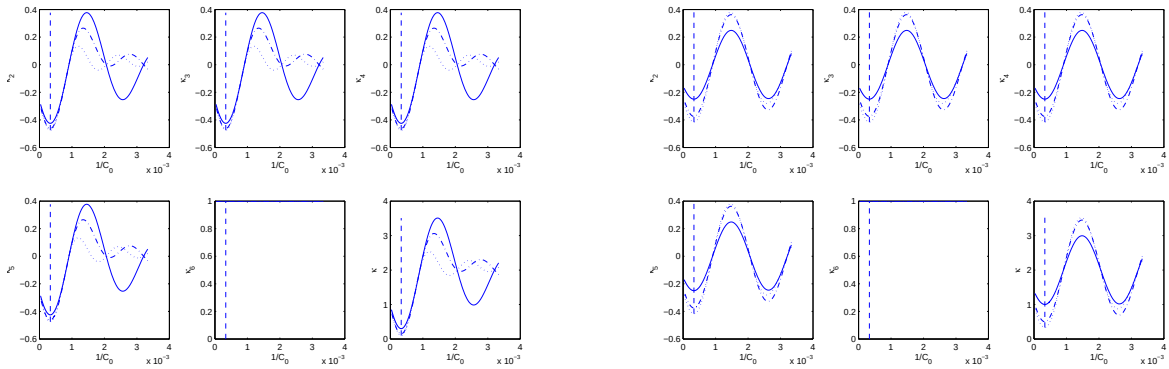

(a) (b)

Figure 8: (a): $\theta^i = 60°$, $\delta_\gamma = 0.1$, $\gamma = 60.1$ Hz, $\eta =$ **20** Hz (——), **40** Hz (-.-.-.-), **60** Hz (.....). The global minimum is at 2998 m/s for all three values of η.
(b): $\theta^i = 60°$, $\delta_\gamma = 0.1$, $\gamma = 60.1$ Hz, $\eta =$ **6** Hz (——), **12** Hz (-.-.-.-), **18** Hz (.....). The global minimum is at 2998 m/s for all three values of η.

The results in fig. 8 show, in agreement with the theoretical prediction A of sect. 6.6, that the position of the global minimum is independent of η and δ_γ. However, the shape of the cost functional does depend on these parameters, with (as in the inverse crime situation) the secondary minima becoming deeper as η is decreased, which fact again underlines the necessity of employing probe radiation whose bandwidth is as large as possible. Since, in this case, there is no discrepancy between Θ^i and θ^i, the retrieval is nose-on the target.

7.2.4 The only uncertain prior is $\mathcal{E}$. Variable η

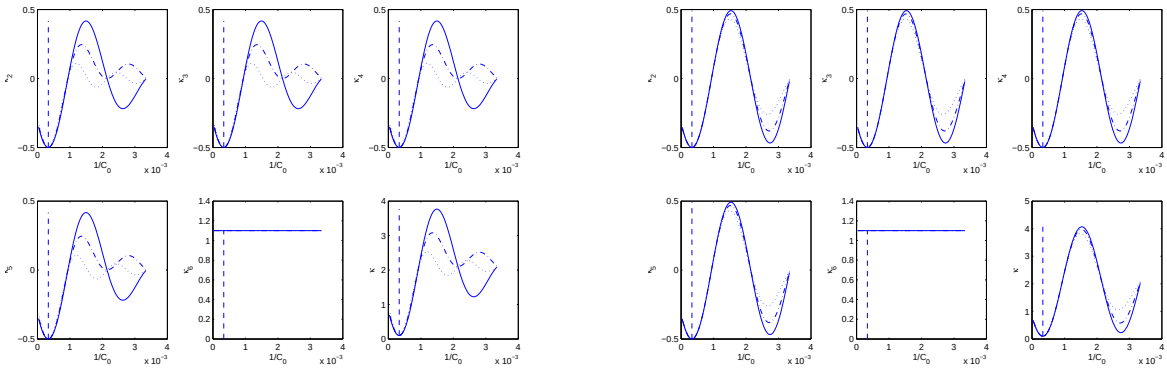

(a) (b)

Figure 9: (a): $\theta^i = 60°$, $\delta_\eta = 0.1$, $\gamma = 60.1$ Hz, $\eta =$ **20** Hz (——), **40** Hz (-.-.-.-), **60** Hz (.....). The global minimum is at 2998 m/s for all three values of η.
(b): $\theta^i = 60°$, $\delta_\eta = 0.1$. $\gamma = 60.1$ Hz, $\eta =$ **6** Hz (——), **12** Hz (-.-.-.-), **18** Hz (.....). The global minimum is at 2998 m/s for all three values of η.

The results in fig. 9 show, in agreement with the theoretical prediction A of sect. 6.6, that the position of the global minimum is independent of η and δ_η. The same remarks as in the previous section hold here as well.

7.2.5 The only uncertain prior is $\mathcal{I}$. Variable ι

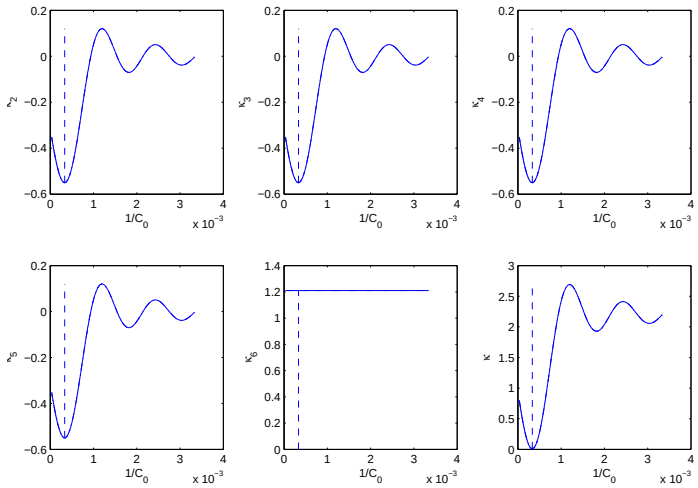

Figure 10: $\theta^i = 60°$. $\delta_\iota = 0.1$. $\gamma = 60.1$ Hz. $\eta = 60$ Hz. $\iota = \mathbf{1} \times \mathbf{10^{-4}}$ m (——), $\mathbf{2} \times \mathbf{10^{-4}}$ m (-.-.-.-), $\mathbf{3} \times \mathbf{10^{-4}}$ m (.....). The target (- - - -) is at 3000 m/s, whereas the global minimum is at 2998 m/s for all three values of $\mathcal{I}$.

The result in fig. 10 shows, in agreement with the theoretical prediction A of sect. 6.6, that the position of the global minimum is independent of ι and δ_ι. This property also applies to the shape of the cost function.

7.2.6 The only uncertain prior is Θ^i. Variable θ^i

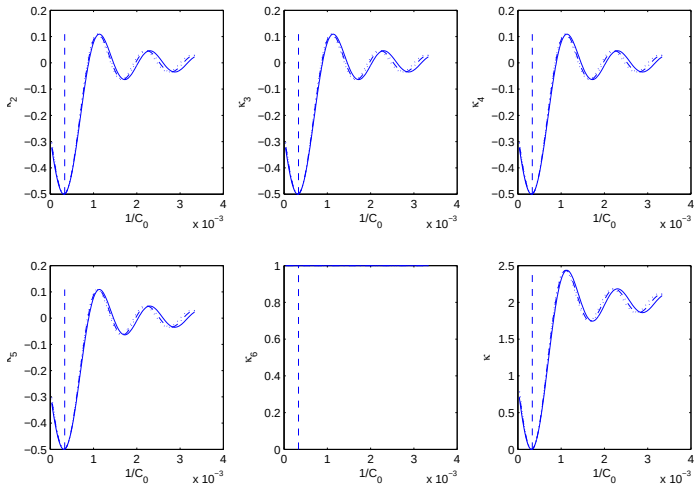

Figure 11: $\delta_{\theta^i} = 0.1$. $\gamma = 60.1$ Hz. $\eta = 60$ Hz. $\theta^i = \mathbf{60}^\circ$ (——), $\mathbf{65}^\circ$ (-.-.-.-), $\mathbf{70}^\circ$ (.....). The target (- - - -) is at 3000 m/s, whereas the global minimum is at 3164 m/s, 3140 m/s and 3111 m/s, for the three values of θ^i respectively.

The result in fig. 11 shows, in agreement with the theoretical prediction A of sect. 6.6, that the position of the global minimum is weakly-independent on θ^i and (for reasonably-small) δ_{θ^i}. This weak dependence is also true as concerns the shape of the component and total cost functions.

7.2.7 The only uncertain prior is X_0. Variable x_0

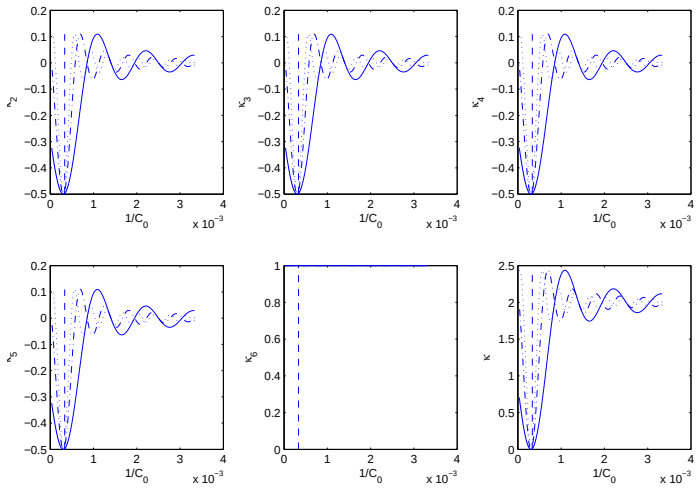

Figure 12: $\delta_{x_0} = 0.1$. $\gamma = 60.1$ Hz. $\eta = 60$ Hz. $x_0 =$ **100** m (——), **200** m (-.-.-.-), **300** m (.....). The target (- - - -) is at 3000 m/s, whereas the global minimum is at 3300 m/s for all three values of x_0.

The result in fig. 12, relative to a situation in which $\delta_{\theta^i} = 0$, shows, in agreement with the theoretical prediction A of sect. 6.6, that the position of the global minimum is independent of x_0 but dependent on δ_{x_0}. However, increasing x_0 increases the number of secondary minima without an effect of deepening the latter.

8 Numerical results for the SPRCFI method employing data registered at one sensor below the ground in a realistic geophysical situation

The following results, relative to a buried sensor, apply to a rectangular excitation spectrum and to the true parameter set: $c_0' = 3000$ m/s, $c_0'' = 0$ km/s, $y_1 = 100$ m, $\theta^i = 60°$, $\iota = 10^{-4}$ m, unless specified otherwise.

8.1 The inverse crime situation

The parameters corresponding to this situation are: $\delta_{x_0} = 0$, $\delta_{y_0} = 0$, $\delta_{y_1} = 0$, $\delta_{\theta^i} = 0$, $\delta_\iota = 0$, $\delta_\alpha = 0$ and $\delta_\beta = 0$.

8.1.1 Variable y_0, relatively-large bandwidth

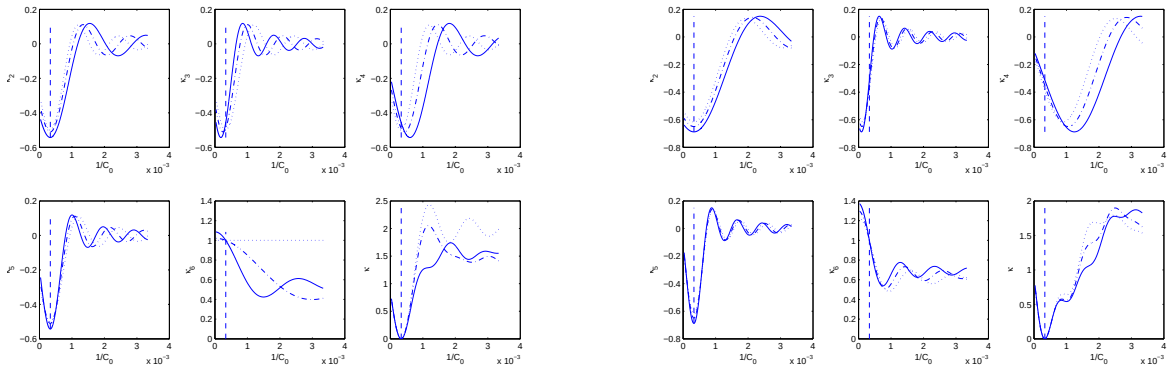

(a) (b)

Figure 13: (a): $\gamma = 60.1$ Hz, $\eta = 60$ Hz, $y_0 = \mathbf{50}$ m (——), **75** m (-.-.-.-), **100** m (.....). The global minimum is at 2998 m/s for all three values of y_0 (3000 m/s for more samples along the $1/C_0$ axis). (b): $\gamma = 60.1$ Hz, $\eta = 60$ Hz, $y_0 = \mathbf{0}$ m (——), **10** m (-.-.-.-), **20** m (.....). The global minimum is at 2998 m/s for all three values of y_0.

The first observation concerning fig. 13, is, in agreement with the predictions of sect. 6.6, that the component cost functions κ_2, κ_3, κ_4, κ_5 (and, in particular, the location of their principal minima) are now generally different one from the other (κ_6 always is different from the other component cost functions), this being true in all the following results pertaining to a buried sensor. This has the effect of introducing supplementary, potentially deep, secondary minima in the total cost function, even in situations in which previously there were no, or few, secondary minima in κ. The results in these two figures show that this effect is all the more pronounced the deeper is the sensor. Note that this is not a consequence of prior uncertainty since we are here in the inverse crime situation.

8.1.2 Variable y_0, relatively-small bandwidth

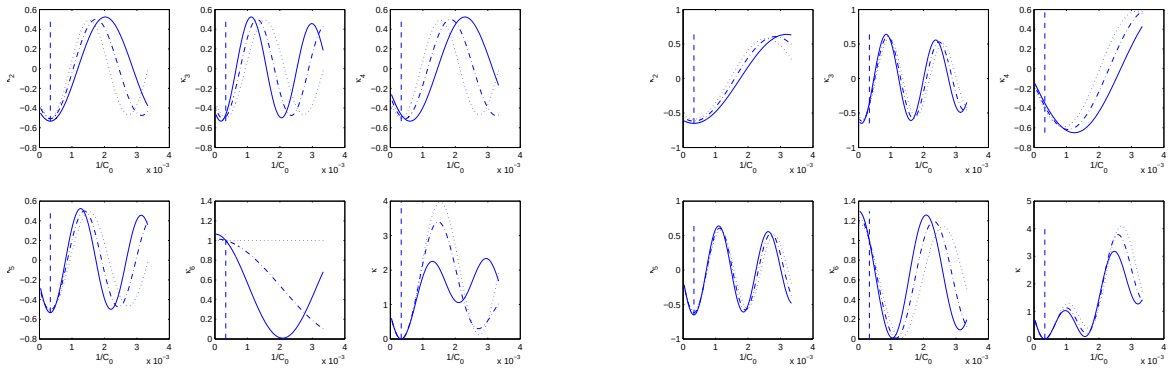

(a) (b)

Figure 14: (a): $\gamma = 60.1$ Hz, $\eta = 6$ Hz, $y_0 =$ **50** m (——), **75** m (-.-.-.-), **100** m (.....). The global minimum is at 2998 m/s for all three values of y_0 (3000 m/s for more samples along the $1/C_0$ axis). (b): $\gamma = 60.1$ Hz, $\eta = 6$ Hz, $y_0 =$ **0** m (——), **10** m (-.-.-.-), **20** m (.....). The global minimum is at 2998 m/s for all three values of y_0.

Fig. 14, shares with fig. 13 the characteristic that the component cost functions κ_2, κ_3, κ_4, κ_5, κ_6 (and, in particular, the location of their principal minima) are now generally different one from the other. This again has the effect of introducing supplementary, potentially deep, secondary minima, an effect that is all the more pronounced the deeper is the sensor, so that for the deepest sensor we nearly obtain a situation in which the global minimum can be located far from $1/c_0$. Note that this is not a consequence of prior uncertainty since we are here in the inverse crime situation, but rather one of sensor burial and near-monochromaticity of the excitation spectrum.

8.2 The (usual) situation in which one or more priors are uncertain

The parameters corresponding to this situation are: $\delta_{x_0} \neq 0$ and/or $\delta_{y_0} \neq 0$ and/or $\delta_{y_1} \neq 0$ and/or $\delta_{\theta^i} \neq 0$ and/or $\delta_\iota \neq 0$ and/or $\delta_\alpha \neq 0$ and/or and $\delta_\beta \neq 0$.

8.2.1 Uncertainty on Y_0. Variable y_0

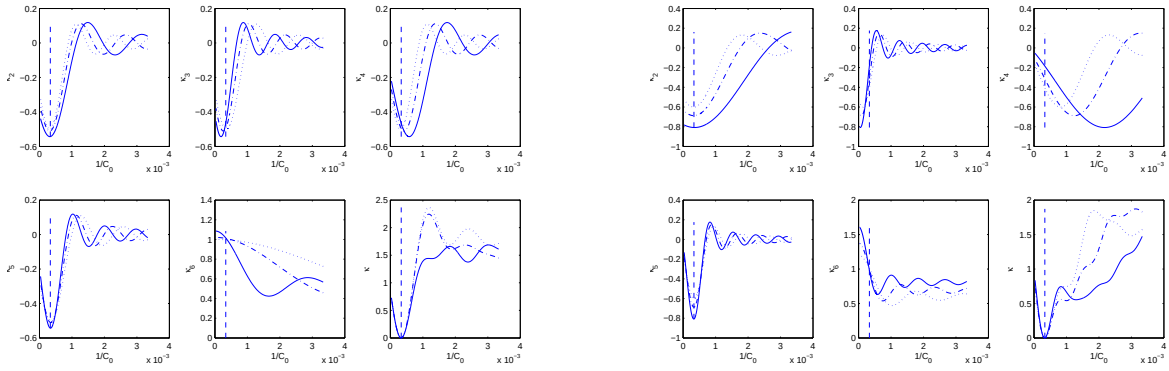

(a) (b)

Figure 15: (a): $\delta_{y_0} = 0.1$, $\gamma = 60.1$ Hz, $\eta = 60$ Hz, $y_0 =$ **50** m (——), **75** m (-.-.-.-), **100** m (.....). The global minimum is at 2998 m/s for all three values of y_0.
(b): $\delta_{y_0} = 0.1$, $\gamma = 60.1$ Hz, $\eta = 60$ Hz, $y_0 = -$**25** m (——), **0** m (-.-.-.-), **25** m (.....). The global minimum is at 2998 m/s for all three values of y_0.

The results in fig. 15, concerning both the component and total cost functions, follow essentially the same pattern of shape changes, and the retrievals occur at the same value c_0, as in sect. 8.1.1 due to the relative smallness of δ_{y_0}.

8.2.2 Uncertainty on Θ^i. Variable y_0

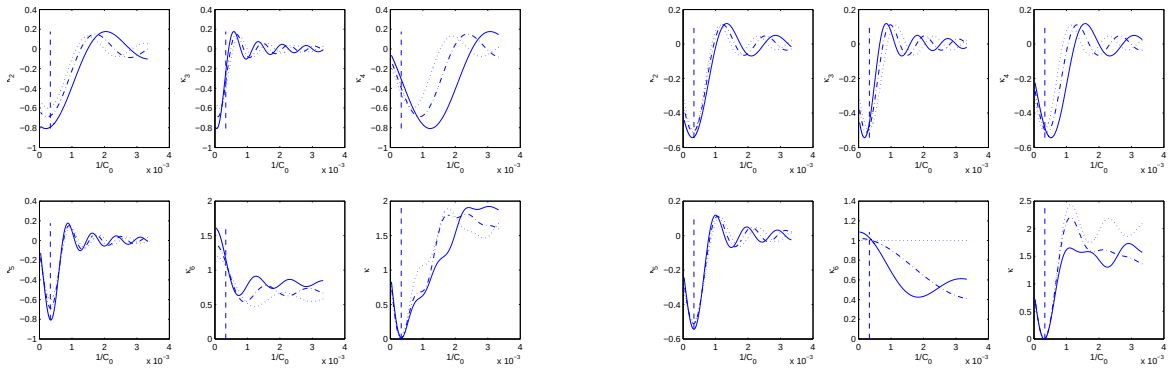

(a) (b)

Figure 16: (a): $\delta_{\theta^i} = 0.1$, $\gamma = 60.1$ Hz, $\eta = 60$ Hz, $y_0 = -\mathbf{25}$ m (——), $\mathbf{0}$ m (-.-.-.-), $\mathbf{25}$ m (.....). The global minimum is at 2916 m/s, 3069 m/s and 3134 m/s for the three values of y_0 respectively. (b): $\delta_{\theta^i} = 0.1$, $\gamma = 60.1$ Hz, $\eta = 60$ Hz, $y_0 = \mathbf{50}$ m (——), $\mathbf{75}$ m (-.-.-.-), $\mathbf{100}$ m (.....). The global minimum is at 3158 m/s, 3164 m/s and 3164 m/s for the three values of y_0 respectively.

The results in fig. 16, concerning both the component and total cost functions, follow essentially the same pattern of shape changes as in sect. 8.1.1. The retrievals occur at values of C_0 that are not very far from c_0 due to the relative smallness of δ_{θ^i}.

8.2.3 Fixed uncertainty of Θ^i, variable uncertainty of $\mathcal{I}$ for two search intervals.

We now turn to the issue of the influence of the choice of search interval. In the preceding figures we deliberately chose this interval of C_0 to be large (in fact: $[3 \times 10^2,\ 3 \times 10^4]$ m/s encompassing the target $c_0 = 3 \times 10^3$ m/s) because we assumed that very little was known a priori as to the actual value of the wavespeed, and even less so as to what value of C_0 would correspond to the global minimum of the cost functional in the presence of prior uncertainties. Choosing a wide search interval is a penalizing operation from at least two points of view: 1) it increases the cost of finding the global minimum of the cost functional κ, and 2) it increases the risk of encountering secondary minima that are generally-annoying features of κ. On the other hand, if the search interval is chosen to be relatively-narrow, we run the risk of either finding no minimum whatsoever (see an example of this in [13]) or simply a local minimum of κ. In either case, the choice of search interval is a crucial aspect of parameter retrieval inverse problems. To illustrate this, we plot, in the following figures, and then in sect. 9, the retrieved value $\widetilde{C_0}$ of C_0 (as obtained from the position of the global minimum in the chosen search interval) versus one of the uncertain priors, for two search intervals.

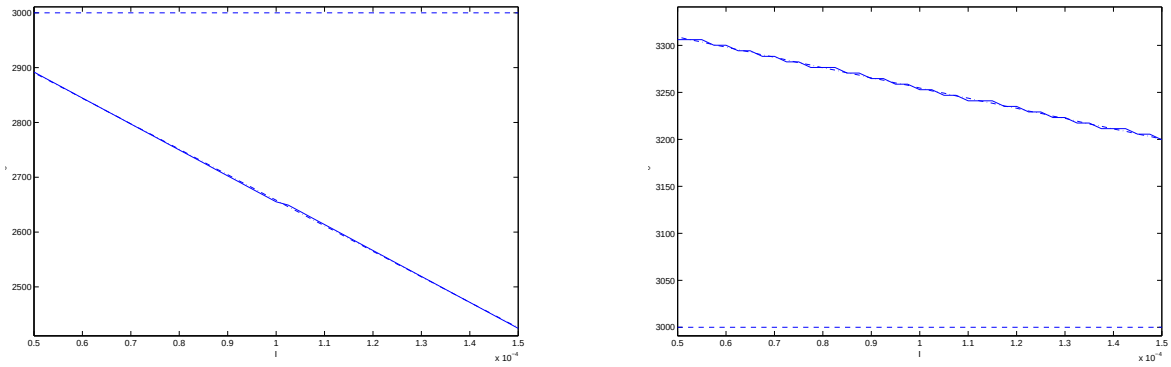

(a) (b)

Figure 17: (a): $X_0 = x_0 = 100$ m, $Y_0 = y_0 = 50$ m, $Y_1 = y_1 = 100$ m, $\theta^i = 60°$, $\Theta^i = \mathbf{50}°$, $\iota = 1 \times 10^{-4}$, $\mathcal{G} = \gamma = 0.05$ Hz, $\mathcal{E} = \eta = 40$ Hz. The target (- - - -) is at 3000 m/s. (——-) corresponds to the search interval $C_0' \in [3 \times 10^2, 3 \times 10^4]$ m/s. (-.-.-.-.) corresponds to the search interval $C_0' \in [1 \times 10^3, 4 \times 10^3]$ m/s.
(b): $X_0 = x_0 = 100$ m, $Y_0 = y_0 = 50$ m, $Y_1 = y_1 = 100$ m, $\theta^i = 60°$, $\Theta^i = \mathbf{70}°$, $\iota = .5 \times 10^{-4}$, $\mathcal{G} = \gamma = 0.05$ Hz, $\mathcal{E} = \eta = 40$ Hz. The target (- - - -) is at 3000 m/s. (——-) corresponds to the search interval $C_0' \in [3 \times 10^2, 3 \times 10^4]$ m/s. (-.-.-.-.) corresponds to the search interval $C_0' \in [1 \times 10^3, 4 \times 10^3]$ m/s.

In fig. 17, we observe that the retrievals are indifferent to the choices of search interval, the reason for this being simply that the global minimum of κ is included in both search intervals. The small difference of the two curves is due to the fact that we chose the same number of discrete samples (in terms of C_0) of κ for the large as for the small search interval. Incidentally, this figure illustrates the fact that the impact of $\mathcal{I}$ uncertainty varies significantly with the uncertainty of Θ^i.

8.2.4 Variable uncertainty of Θ^i for two search intervals. No uncertainty on the other priors. Sensors at three depths.

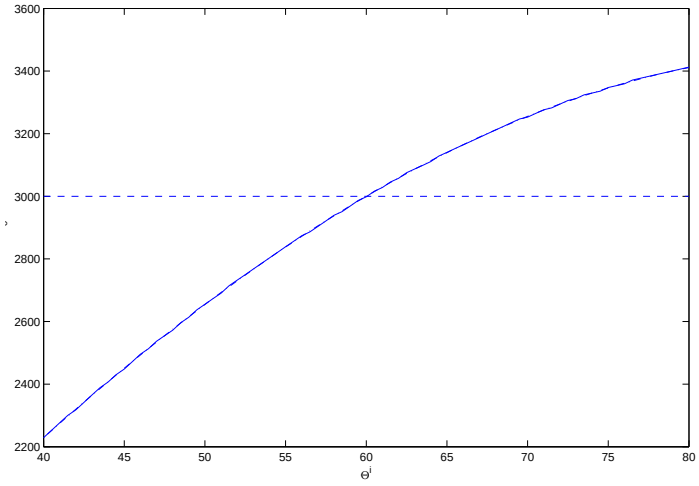

Figure 18: $X_0 = x_0 = 100$ m. $Y_0 = y_0 = \mathbf{70}$ m. $Y_1 = y_1 = 100$ m. $\theta^i = 60°$. $\mathcal{I} = \iota = 1 \times 10^{-4}$. $\mathcal{G} = \gamma = 0.05$ Hz. $\mathcal{E} = \eta = 40$ Hz. The target (- - - -) is at 3000 m/s. (——-) corresponds to the search interval $C_0' \in [3 \times 10^2, 3 \times 10^4]$ m/s. (-.-.-.-.) corresponds to the search interval $C_0' \in [1 \times 10^3, 4 \times 10^3]$ m/s. The same curves are obtained for $Y_0 = y_0 = \mathbf{90}$ m and $Y_0 = y_0 = \mathbf{100}$ m.

In fig. 18, we observe once again that the retrievals are indifferent to the choices of search interval, the reason for this being simply that the global minimum of κ is included in both search intervals. Incidentally, this figure (together with two others not shown here) illustrates the fact that the retrievals vary significantly with the uncertainty of Θ^i, but not at all with $Y_0 = y_0$.

8.2.5 Variable uncertainty of $\mathcal{G}$ for two search intervals. Two fixed uncertainties on Θ^i. No uncertainty on the other priors.

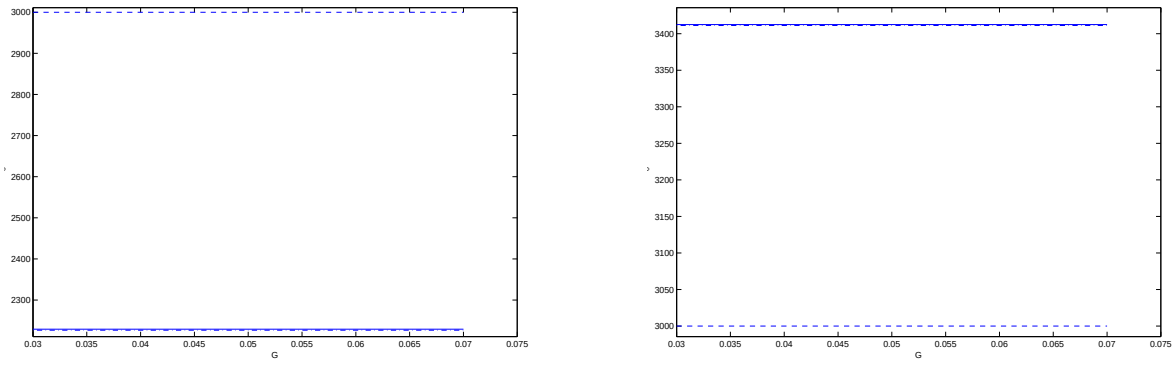

(a) (b)

Figure 19: (a): $X_0 = x_0 = 100$ m, $Y_0 = y_0 = 100$ m, $Y_1 = y_1 = 100$ m, $\theta^i = 60°$, $\Theta^i = \mathbf{40}°$, $\mathcal{I} = \iota = 1 \times 10^{-4}$, $\gamma = 0.05$ Hz, $\mathcal{E} = \eta = 40$ Hz. The target (- - - -) is at 3000 m/s. (——-) corresponds to the search interval $C_0' \in [3 \times 10^2, 3 \times 10^4]$ m/s. (-.-.-.-.) corresponds to the search interval $C_0' \in [1 \times 10^3, 4 \times 10^3]$ m/s.
(b): $X_0 = x_0 = 100$ m, $Y_0 = y_0 = 100$ m, $Y_1 = y_1 = 100$ m, $\theta^i = 60°$, $\Theta^i = \mathbf{80}°$, $\mathcal{I} = \iota = 1 \times 10^{-4}$, $\gamma = 0.05$ Hz, $\mathcal{E} = \eta = 40$ Hz. (——-) corresponds to the search interval $C_0' \in [3 \times 10^2, 3 \times 10^4]$ m/s. (-.-.-.-.) corresponds to the search interval $C_0' \in [1 \times 10^3, 4 \times 10^3]$ m/s.

In fig. 19, the retrievals are found, once again, to be indifferent to the choices of search interval, the reason for this being simply that the global minimum of κ is included in both search intervals. Incidentally, this figure illustrates the fact that the retrievals do not vary at all with the uncertainty of $\mathcal{G}$, be it for one, or for the other values of $\Theta^i \neq \theta^i$.

8.2.6 Variable uncertainty of $\mathcal{E}$ for two search intervals. Fixed uncertainty on Θ^i. No uncertainty on the other priors. Sensors at three depths.

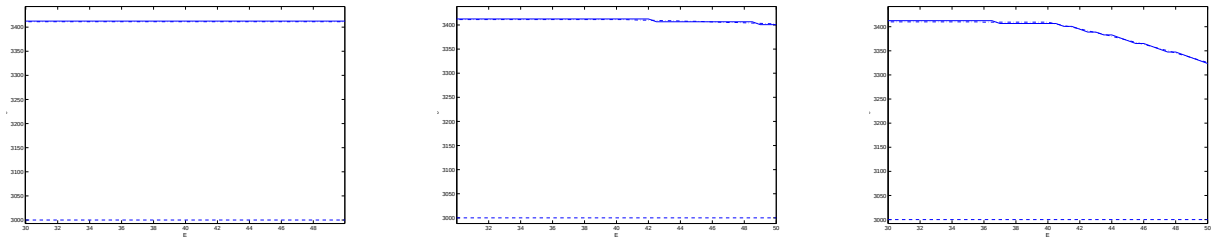

(a) (b) (c)

Figure 20: (a): $X_0 = x_0 = 100$ m, $Y_0 = y_0 = \mathbf{100}$ m, $Y_1 = y_1 = 100$ m, $\theta^i = 60°$, $\Theta^i = 80°$, $\mathcal{I} = \iota = 1 \times 10^{-4}$, $\mathcal{I} = 1 \times 10^{-4}$, $\mathcal{G} = \gamma = 0.05$ Hz, $\eta = 40$ Hz. (——-) corresponds to the search interval $C_0' \in [3 \times 10^2, 3 \times 10^4]$ m/s. (-.-.-.-.) corresponds to the search interval $C_0' \in [1 \times 10^3, 4 \times 10^3]$ m/s.
(b): $X_0 = x_0 = 100$ m, $Y_0 = y_0 = \mathbf{70}$ m, $Y_1 = y_1 = 100$ m, $\theta^i = 60°$, $\Theta^i = 80°$, $\mathcal{I} = \iota = 1 \times 10^{-4}$, $\mathcal{I} = 1 \times 10^{-4}$, $\mathcal{G} = \gamma = 0.05$ Hz, $\eta = 40$ Hz. (——-) corresponds to the search interval $C_0' \in [3 \times 10^2, 3 \times 10^4]$ m/s. (-.-.-.-.) corresponds to the search interval $C_0' \in [1 \times 10^3, 4 \times 10^3]$ m/s.
(c): $X_0 = x_0 = 100$ m, $Y_0 = y_0 = \mathbf{10}$ m, $Y_1 = y_1 = 100$ m, $\theta^i = 60°$, $\Theta^i = 80°$, $\mathcal{I} = \iota = 1 \times 10^{-4}$, $\mathcal{I} = 1 \times 10^{-4}$, $\mathcal{G} = \gamma = 0.05$ Hz, $\eta = 40$ Hz. (——-) corresponds to the search interval $C_0' \in [3 \times 10^2, 3 \times 10^4]$ m/s. (-.-.-.-.) corresponds to the search interval $C_0' \in [1 \times 10^3, 4 \times 10^3]$ m/s.

In fig. 20, once again, the retrievals are found to be indifferent to the choices of search interval, the reason for this being simply that the global minimum of κ is included in both search intervals. Incidentally, these figures illustrate the fact that the retrievals do not vary at all with the uncertainty of $\mathcal{E}$ as long as the sensor is on or near (but below) the ground, but do vary somewhat with $\mathcal{E}$ as soon as $Y_0 = y_0 = 10$ m.

Lest we be fooled by these results pointing to the apparent independence of the retrievals on the choices of search interval, we now turn to a case in which the situation is entirely different.

9 Numerical results for the SPRCFI method employing data registered at one sensor below the ground in a less-realistic (high-frequency) geophysical situation

The results here apply to a rectangular, but now relatively-high frequency excitation spectrum, not usually encountered in natural seismic signals, but chosen to illustrate some pathological features of cost functions that can be encountered when the underground is probed by radiation from non-natural (e.g., vibrator [24]) sources. Again, the true parameter set is: $c_0' = 3000$ m/s, $c_0'' = 0$ km/s, $y_1 = 100$ m, $\theta^i = 60°$, $\iota = 10^{-4}$ m, unless specified otherwise.

9.1 The (usual) situation in which one or more priors are uncertain

The parameters corresponding to this situation are: $\delta_{x_0} \neq 0$ and/or $\delta_{y_0} \neq 0$ and/or $\delta_{\theta^i} \neq 0$ and/or $\delta_\iota \neq 0$ and/or $\delta_\alpha \neq 0$ and/or and $\delta_\beta \neq 0$.

9.1.1 Uncertainty on Y_0. Variable y_0

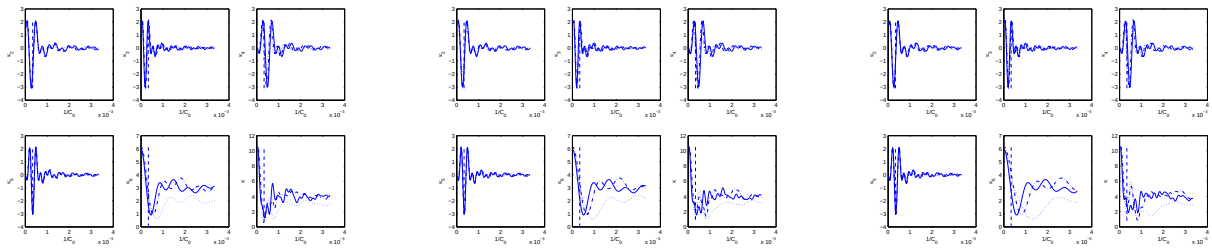

(a) (b) (c)

Figure 21: (a): $\delta_{\theta^i} = 0.13333$, $\delta_{y_0} = \mathbf{0.1}$, $\gamma = 380$ Hz, $\eta = 180$ Hz, $y_0 = 50$ m (——), 57.5 m (-.-.-.-), 65 m (.....). The global minimum is at 2735 m/s, 2865 m/s, 3140 m/s, for the three values of y_0 respectively.
(b): $\delta_{\theta^i} = 0.13333$, $\delta_{y_0} = \mathbf{0.2}$, $\gamma = 380$ Hz, $\eta = 180$ Hz, $y_0 = 50$ m (——), 57.5 m (-.-.-.-), 65 m (.....). The global minimum is at 2602 m/s, 1220 m/s, 3161 m/s, for the three values of y_0 respectively.
(c): $\delta_{\theta^i} = 0.13333$, $\delta_{y_0} = \mathbf{0.3}$, $\gamma = 380$ Hz, $\eta = 180$ Hz, $y_0 = 50$ m (——), 57.5 m (-.-.-.-), 65 m (.....). The global minimum is at 1199 m/s, 1208 m/s, 3185 m/s, for the three values of y_0 respectively.

With regard to fig. 21, we are now in the situation in which each of the component cost functions is dominated by the principal pulse of the sinc function whose position is rather well separated from one component to the other. This has the effect of producing four to five (related to the number of component cost functions) deep minima in the total cost functional κ. As the uncertainty concerning the depth of the sensor, as well as the depth itself, are varied, the way these component cost functions combine varies also, so as to promote (i.e., increase the depth of) one of these component troughs at the expense of the others. As the location of the extrema of the

various sinc functions can be rather far-removed from $1/c_0$, the retrievals, corresponding to the global minimum of κ, can turn out to be (as observed) far-removed from the target. Note should also be taken of the important influence of the deep trough of κ_6 in shaping the total cost functional κ.

9.1.2 Uncertainty of Θ^i. The effect of changing the search interval.

In figs. 22-23, we change the pictorial organization. The top panel corresponds to the component cost functions κ_1, κ_2, κ_3, κ_4, κ_5, κ_6 as a function of $1/C_0$, whereas the bottom panel corresponds to κ as a function of $1/C_0$. Each figure concerns only a single choice of true and prior parameters as well as a single choice of search interval. The last figure in this section, i.e., fig. 24, depicts the retrievals as a function of a prior for two choices of search intervals.

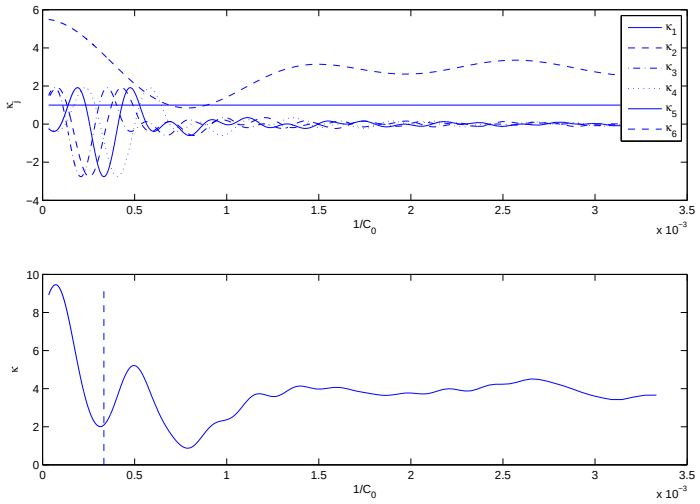

Figure 22: $X_0 = x_0 = 100$ m. $Y_0 = y_0 = 60$ m. $Y_1 = y_1 = 100$ m. $\theta^i = 60°$, $\Theta^i = 76°$. $\mathcal{I} = \iota = 10^{-4}$ m. $\gamma = 380$ Hz. $\eta = 180$ Hz. (——-) corresponds to the search interval $C_0' \in [\mathbf{3 \times 10^2}, \mathbf{3 \times 10^4}]$ m/s. The target is at 3000 m/s.

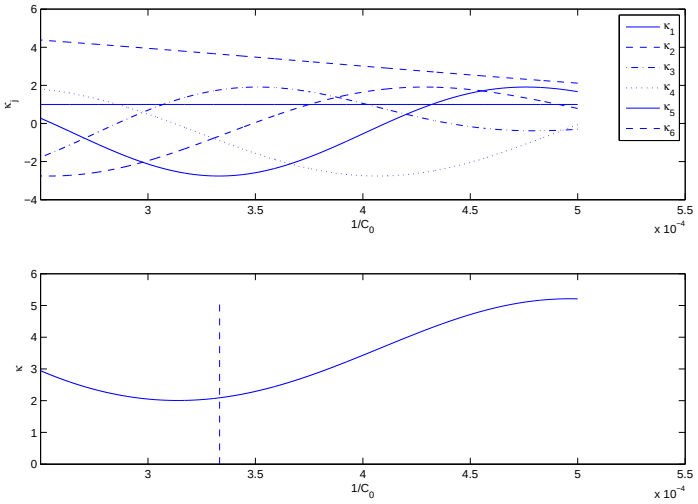

Figure 23: $X_0 = x_0 = 100$ m. $Y_0 = y_0 = 60$ m. $Y_1 = y_1 = 100$ m. $\theta^i = 60°$, $\Theta^i = 76°$. $\mathcal{I} = \iota = 10^{-4}$ m. $\gamma = 380$ Hz. $\eta = 180$ Hz. (——-) corresponds to the search interval $C_0' \in [\mathbf{2 \times 10^3}, \mathbf{4 \times 10^3}]$ m/s. The target is at 3000 m/s.

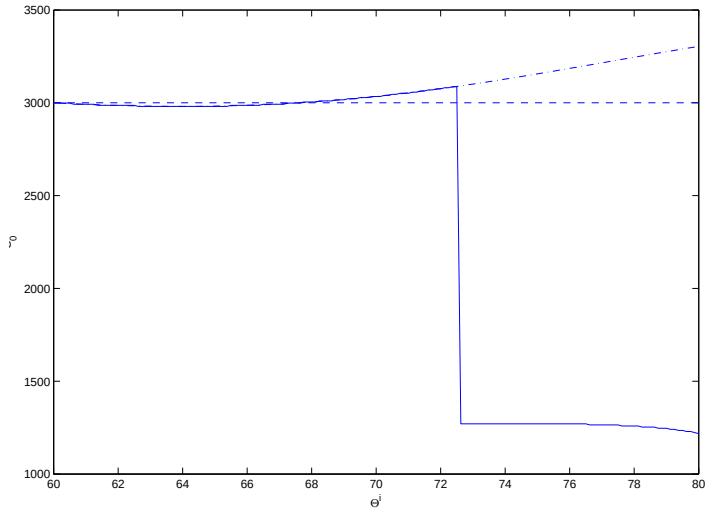

Figure 24: Location of the global minimum as a function of Θ^i. $X_0 = x_0 = 100$ m. $Y_0 = y_0 = 60$ m. $Y_1 = y_1 = 100$ m. $\theta^i = 60°$. $\mathcal{I} = \iota = 10^{-4}$ m. $\gamma = 380$ Hz. $\eta = 180$ Hz. (——-) corresponds to the search interval $C_0' \in [\mathbf{3 \times 10^2}, \mathbf{3 \times 10^4}]$ m/s (first of two preceding graphs). (-.-.-.-.) corresponds to the search interval $C_0' \in [\mathbf{2 \times 10^3}, \mathbf{4 \times 10^3}]$ m/s (second of two preceding graphs). The target is at 3000 m/s (- - - -).

In fig. 22, we observe that, due to the presence of the deep trough in κ_6, the global minimum is at 1270 m/s, which is very far from the target. However, there also exists a deep, secondary minimum, much closer to the target. Fig. 23 differs from fig. 22 by the fact that the search interval is much smaller, the effect being to eliminate the candidate minimum at 1270 m/s in favor of the (formerly secondary, now global) minimum at 3185 m/s, which is reasonably near the target. In figs. 22-23, the value of the prior Θ^i was fixed, whereas in fig. 24, it is varied and the position of the global minimum of κ is recorded as obtained for the two different search intervals of the two previous figures. The notable feature is the staircase-like behavior of the curve (——), relative to the larger search interval, which is another manifestation of *prior uncertainty − induced retrieval instability* previously discovered in [18].

We now consider whether the employment of multi-sensor data enables to resolve this non-uniqueness issue.

10 Theoretical aspects of the SPRCFI method for multisensor data

10.1 Definition of the SPRCFI cost functional for single sensor data and rectangular excitation spectrum

We now assume that the data is registered at several point-like sensors located at (x_{01}, y_{01}), (x_{012}, y_{02}),...,(x_{0N}, y_{0N}) beneath or on the ground. We include the coordinates $\mathbf{x}_{0n}$ within the set $\mathbf{q}_n$ and their perhaps-uncertain equivalents $\mathbf{X}_{0n}$ within the set $\mathbf{Q}_n$. We adopt the shorthand

notation: $K = K(\mathbf{R}, \mathbf{Q}_n)$, $U_n(\omega) = U_0(\mathbf{R}, \mathbf{Q}_n, \omega)$, $u_n(\omega) = u_0(\mathbf{r}, \mathbf{q}_n, \omega)$. Eqs. (24)-(26) still apply, but the definition of the normalized cost functional (formerly (52)) is now

$$\kappa = \frac{\sum_{n=1}^{N} \int_{-\infty}^{\infty} \|u_n(\omega) - U_n(\omega)\|^2 d\omega}{\sum_{n=1}^{N} \int_{-\infty}^{\infty} \|u_n(\omega)\|^2 d\omega} \ . \tag{52}$$

Since the spectrum $s(\omega)$ of u was assumed to be of finite bandwidth $[\alpha, \beta]$, it is reasonable to assume that the spectrum $S(\omega)$ of U be also of finite (but not necessarily the same) bandwidth $[\mathcal{A}, \mathcal{B}]$, so that the integrals in the previous expression are necessarily over the finite bandwidth $[\omega_b, \omega_e]$, the issue of the relation of ω_b to α, $\mathcal{A}$ and of ω_e to β, $\mathcal{B}$ being as previously. Consequently,

$$\kappa = \frac{\sum_{n=1}^{N} \int_{\omega_b}^{\omega_e} \|u_n(\omega) - U_n(\omega)\|^2 d\omega}{\sum_{n=1}^{N} \int_{\omega_b}^{\omega_e} \|u_n(\omega)\|^2 d\omega} \ . \tag{53}$$

The sums in this expression makes it difficult to analyze the cost functional in the manner previously adopted for the single-sensor situation, so that we shall content ourselves with numerical illustrations of the hoped-for property that multisensor data has the beneficial effect of deepening the already deepest trough, while leveling out the other troughs, of the single-sensor cost function.

11 Numerical results for the SPRCFI method employing data registered at several sensors on the ground in a realistic geophysical situation

The following results again apply to a rectangular excitation spectrum and to the true parameter set: $c_0' = 3000$ m/s, $c_0'' = 0$ km/s, $y_1 = 100$ m, $\theta^i = 60°$, $\iota = 10^{-4}$ m, $\alpha = .05$ Hz, $\beta = 40$ Hz, unless specified otherwise.

11.1 Inverse crime situation

The parameters corresponding to this situation are: $X_0 = x_0$, $Y_0 = y_0$, $\Theta^i = \theta^i$, $\mathcal{A} = \alpha$ and $\mathcal{B} = \beta$.

11.1.1 Variable number of sensors.

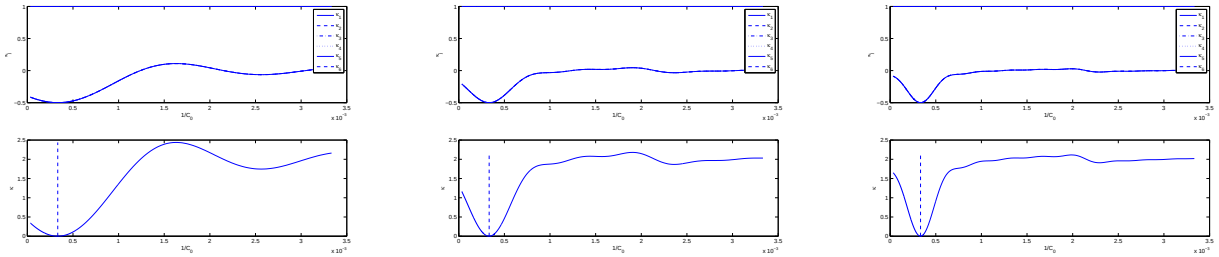

(a) (b) (c)

Figure 25: (a): One sensor at $x_0 =$ **100** m. The target is at 3000 m/s, whereas the global minimum is at 3001 m/s (3000 m/s for more sampling points along $1/C_0$ axis).
(b): Three sensors at $x_0 =$ **100**, **200**, **300** m. The global minimum is at 3001 m/s.
(c): Five sensors at $x_0 =$ **100**, **200**, **300**, **400**, **500** m. The global minimum is at 3001 m/s.

The results in fig. 25, , once again relative to a low-frequency situation, now of several equally-spaced sensors on the ground whose positions are certain, show that increasing the number of sensors has the favorable effect of narrowing and deepening the principal trough of κ while rendering relatively-less deep the secondary minimum.. This effect is obtained without affecting the quality of the retrieval, i.e., the position of the global minimum of κ is c_0 whatever the number of sensors.

11.2 Non-inverse crime situation

The parameters corresponding to this situation are: $X_{0n} \neq x_0$ and/or $\Theta^i \neq \theta^i$, $Y_0 = y_0$, $\mathcal{A} = \alpha$ and $\mathcal{B} = \beta$.

11.2.1 Variable number of sensors. $X_{0n} = x_0 + 10$ m, $\Theta^i = \theta^i$, $\mathcal{I} = \iota$.

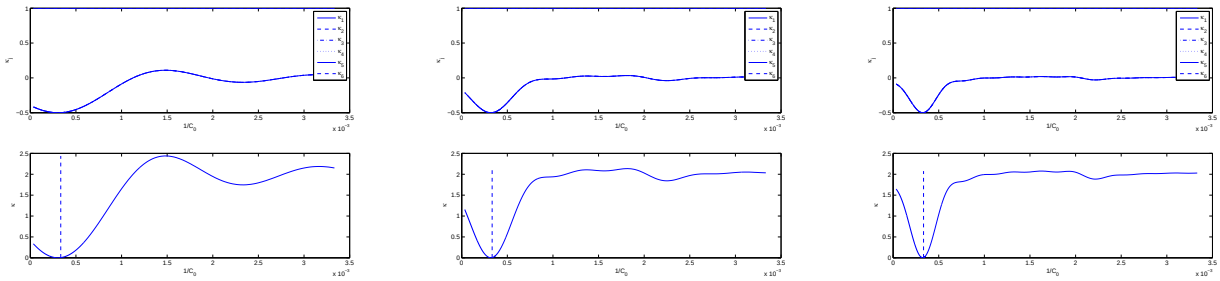

(a) (b) (c)

Figure 26: (a): One sensor at $x_0 =$ **100** m. The global minimum is at 3301 m/s.
(b): Three sensors at $x_0 =$ **100**, **200**, **300** m. The global minimum is at 3129 m/s.
(c): Five sensors at $x_0 =$ **100**, **200**, **300**, **400**, **500** m. The global minimum is at 3083 m/s.

Fig. 26 is relative to an increasing number of sensors on the ground and low-frequency probe radiation. Now, the positions of the sensors are uncertain by a fixed amount. We see that the previously-found beneficial effects of increasing the number of sensors is maintained, but with retrievals that depend on the uncertainty of the positions of the sensors. However, the retrieval error does seem to diminish with the increase of the number of sensors.

11.2.2 Variable number of sensors. $X_0 = x_0$, $\Theta^i = 68°$, $\mathcal{I} = \iota$.

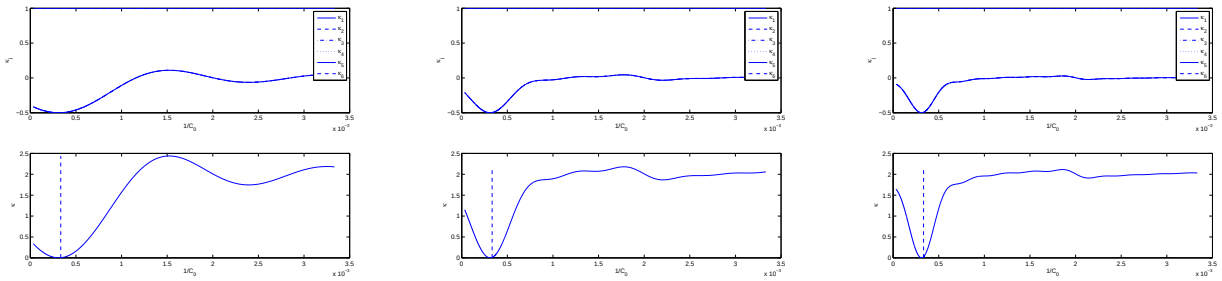

(a) (b) (c)

Figure 27: (a): One sensor at $x_0 = \mathbf{100}$ m. The target is at 3000 m/s, whereas the global minimum is at 3211 m/s.
(b): Three sensors at $x_0 = \mathbf{100}$, $\mathbf{200}$, $\mathbf{300}$ m. The global minimum is at 3211 m/s.
(c): Five sensors at $x_0 = \mathbf{100}$, $\mathbf{200}$, $\mathbf{300}$, $\mathbf{400}$, $\mathbf{500}$ m. The global minimum is at 3211 m/s.

Fig. 27, which is for increasing number of sensors on the ground and low-frequency probe radiation, applies now to the case in which Θ^i is the uncertain prior. We saw previously (for one sensor) that this produces a shift in the location of the global minimum of κ; here we see that the beneficial effects of increasing the number of sensors is maintained without affecting the amount of this shift. Thus, by comparison with fig. 26, the changing position of the global minimum is a consequence of the uncertainty of the positions of the sensors, not of the uncertainty of Θ^i.

11.2.3 Variable number of sensors. $\mathcal{I} = \iota$. Uncertain priors $X_{0n} = x_0 + 10$ m and $\Theta^i = 68°$.

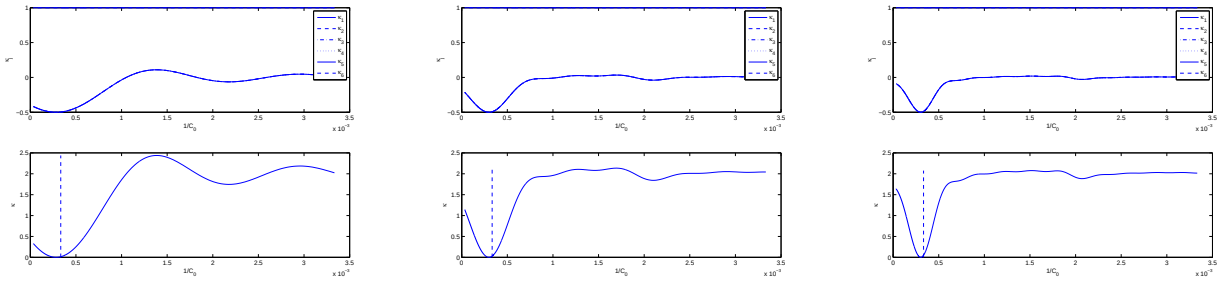

(a) (b) (c)

Figure 28: (a): One sensor at $x_0 = \mathbf{100}$ m. The global minimum is at 3534 m/s.
(b): Three sensors at $x_0 = \mathbf{100}$, $\mathbf{200}$, $\mathbf{300}$ m. The global minimum is at 3351 m/s.
(c): Five sensors at $x_0 = \mathbf{100}$, $\mathbf{200}$, $\mathbf{300}$, $\mathbf{400}$, $\mathbf{500}$ m. The global minimum is at 3301 m/s.

Fig. 28 applies to an increasing number of equally-spaced sensors on the ground for fixed uncertainty on the X_0 of each sensor and fixed uncertainty on Θ^i. Once again, it is seen that increasing the number of sensors has the favorable effect of narrowing and deepening the principal trough of κ, gradually shifting and stabilizing the position of the global minimum, while rendering relatively-less deep the secondary minimum of K.

12 Numerical results for the SPRCFI method employing data registered at several sensors below the ground in a high-frequency situation

The following results again apply to several sensors below the ground, a high-frequency rectangular excitation spectrum and to the true parameter set: $c_0' = 3000$ m/s, $c_0'' = 0$ km/s, $y_1 = 100$ m, $\theta^i = 60°$, $\iota = 10^{-4}$ m, $\alpha = 100$ Hz, $\beta = 280$ Hz, unless specified otherwise.

12.1 Non-inverse crime situation

The parameters corresponding to this situation are: $X_0 = x_0$, $Y_0 \neq x_0$ and/or $\Theta^i \neq \theta^i$, $Y_1 = y_1$, $\mathcal{A} = \alpha$ and $\mathcal{B} = \beta$.

12.1.1 Variation of the number of vertical sensors for fixed prior uncertainties on Y_{0j} m at each sensor and Θ^i.

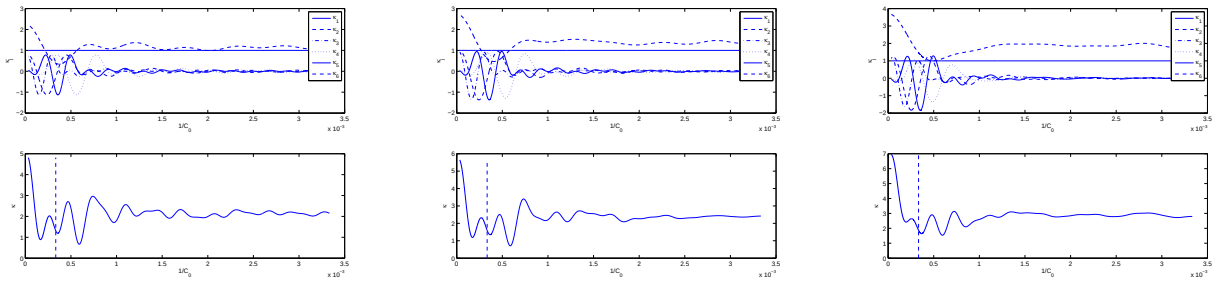

(a) (b) (c)

Figure 29: (a): $\theta^i = 60°$, $\Theta^i = 68°$, $Y_0 = y_0 + 15$ m. One sensor at $X_0 = x_0 = 100$ m, $y_0 = \mathbf{30}$ m. The global minimum is at 1691 m/s.
(b): $\theta^i = 60°$, $\Theta^i = 68°$, $Y_0 = y_0 + 15$ m. Two sensors at $X_0 = x_0 = 100$ m, $Y_0 = y_0 + 15$ m. $y_0 = \mathbf{30}, \mathbf{40}$ m. The global minimum is at 1703 m/s.
(c): $\theta^i = 60°$, $\Theta^i = 68°$, $Y_0 = y_0 + 15$ m. Four sensors at $X_0 = x_0 = 100$ m, $y_0 = \mathbf{30}, \mathbf{40}, \mathbf{50}, \mathbf{60}$ m. The global minimum is at 1680 m/s.

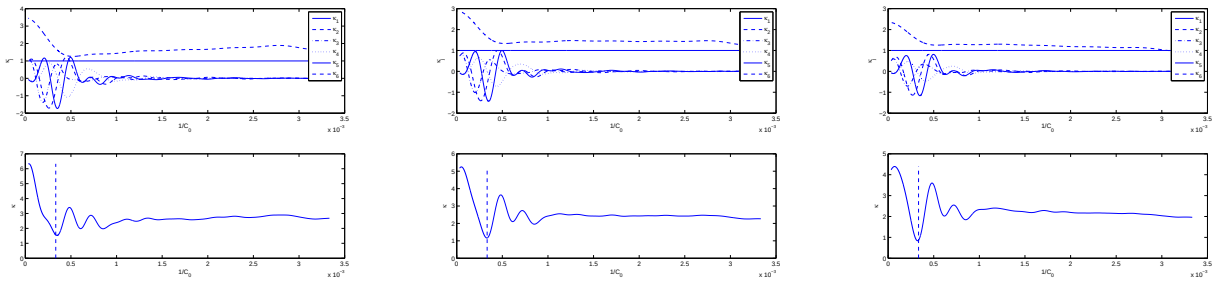

(a) (b) (c)

Figure 30: (a): $\theta^i = 60°$, $\Theta^i = 68°$, $Y_0 = y_0 + 15$ m. Five sensors at $X_0 = x_0 = 100$ m, $y_0 = \mathbf{30}, \mathbf{40}, \mathbf{50}, \mathbf{60}, \mathbf{70}$ m. The global minimum is at 2879 m/s.
(b): $\theta^i = 60°$, $\Theta^i = 68°$, $Y_0 = y_0 + 15$ m. Six sensors at $X_0 = x_0 = 100$ m, $y_0 = \mathbf{30}, \mathbf{40}, \mathbf{50}, \mathbf{60}, \mathbf{70}, \mathbf{80}$ m. The global minimum is at 3028 m/s.
(c): $\theta^i = 60°$, $\Theta^i = 68°$, $Y_0 = y_0 + 15$ m. Seven sensors at $X_0 = x_0 = 100$ m, $y_0 = \mathbf{30}, \mathbf{40}, \mathbf{50}, \mathbf{60}, \mathbf{70}, \mathbf{80}, \mathbf{90}$ m. The global minimum is at 3100 m/s.

The results in figs. 29-30 apply to the situation in which the number of sensors, equally-spaced along a vertical line, is varied and the vertical position prior of each sensor is uncertain by the amount of 15 m. We observe that, for up to four sensors, the position of the global minimum of the cost functional K is far-removed from the target value c_0. For five sensors, the situation changes radically since the position of the global minimum is near the target value. For six or more sensors, the position of the global minimum gradually converges to what appears to be the right location (considering that the incident angle is uncertain).

13 Conclusion

This investigation, devoted to one of the simplest seismic inverse problems (IP) concerning the retrieval of a single parameter from noise-free data, showed, above all, that the issues of what form the cost functional takes (i.e., number of minima and depth of the primary and secondary minima in the chosen search interval, optimal choice of search interval, dependence on the central frequency and bandwidth of the excitation spectrum) and where its global minimum is located (as a function of the search interval, the ten true parameters and the nine priors with varying uncertainty) is far from being simple.

More precisely, the following was accomplished.
1- We (re-)introduced the spectral response (frequency domain) cost functional inversion (SPRCFI) method as a useful alternative to the signal response (time domain) (SIRCFI) method (both being variants of the full-waveform inversion (FWI) technique) for solving typical seismic parameter retrieval problems.
2- We (re-)demonstrated the theoretical equivalence of the SPRCFI and SIRCFI methods.
3- We showed that the SPRCFI (and thus the SIRCFI) cost function(s) can exhibit multiple deep minima, even when the inverse crime is committed, and more often when the inverse crime is not committed.

4- We explained why these multiple minima can occur, notably due to the occurrence of deep minima in the component cost functions.
5- We found algebraic expressions for the location, but unfortunately not the depth, of the principal minima of the component cost functions (related in generally-complex manner to that of the total cost function) as a (nonlinear) function of the true and nuisance parameters of the retrieval problem,
6- We explained why some parameter retrieval problems seem to lead to single-minimum cost functions (this being essentially due to low-frequency probe radiation and/or relatively-narrow search intervals), in apparent contradiction with the notoriously ill-posed nature of IP,
7- We showed that multiple-minima cost functions are at least partly the result of small bandwidth and/or high central frequency probe radiation (when such high frequencies are available)
8- We explained how retrieval error depends on the uncertainty of the parameters of the spectrum and spatial aspects of the probe radiation as well as on the positions of the sensors (we qualify a parameter as being uncertain by the fact that its assigned value, resulting from experiment, guessing or borrowing from a published result, is incorrect in a sense akin to systematic measurement error).
9- We discussed how to deal with multiple-minima cost functions (either in the inverse crime or non-inverse crime situations), notably by increasing the number of sensors and properly choosing their locations.
10- We discussed the issue of whether the global minimum of a cost functional always indicates the "best" solution of the IP, notably in the presence of prior uncertainty.
11- We discussed the related issue of how the choice of search interval affects the existence, uniqueness and stability of the retrieval.

The results obtained herein suggest that if more-complicated, more realistic, seismic inverse problems (involving many parameters, a host of which are priors) be treated by FWI techniques, then:
1) it is probable that the recommendations obtained for our simpler problem as to the interest of employing relatively low central frequency, wide bandwidth probe radiation (notably when these parameters can be chosen such as with non-natural sources), more than one sensors placed on the ground rather than underground, and search spaces that are neither too large, nor too narrow, may still be appropriate;
2) efforts should be devoted to taking into account prior uncertainties, notably to avoid committing the inverse crime when employing synthetic data, to estimate the effect of prior uncertainty on retrieval error, and to widen the search space for prior uncertainties that are larger;
3) it would be useful to depict, if possible, either mathematically or graphically (as we have done), the cost functionals that are generated during the inversion process in order to reduce the risk of obtaining retrievals that either correspond to secondary minima or to global minima of the cost functional that are badly-located due to the choice of an improper search space.

References

[1] Averill M.G., *A lithospheric investigation of the Southern Rio Grande Rift*, Phd thesis, Univ. Texas El Paso (2007).

[2] Bermani E., Boni A., Kerhet A., and Massa A. *Kernels evaluation of SVM-based estimators for inverse scattering problems*, Prog.Electromag.Res., 53, 167-188 (2005).

[3] Buchanan J., Gilbert R., Wirgin A. and Xu Y., *Depth sounding: an illustration of some of the pitfalls of inverse scattering problems*, Math.Comput.Model., 35, 1315-1354 (2002).

[4] Cervelli P., Murray M.H., Segall P., Y. Aoki Y. and T. Kato T. *Estimating source parameters from deformation data, with an application to the March 1997 earthquake swarm off the Izu Peninsula, Japan*, J.Geophys.Res. B, 106, 11217-11237 (2001).

[5] Delprat-Jannaud F. and Lailly P., *A fundamental limitation for the reconstruction of impedance profiles from seismic data*, Geophys., 70, R1-R14, (2005).

[6] Deng H.L. and Scales J.A., *Characterizing the topography of multi-dimensional energy landscapes*, arXiv:1405.2948 [cs.NA] (2014).

[7] Fernndez Martnez J.L., Fernndez Muiz M.Z. and Tompkins M.J. *On the topography of the cost functional in linear and nonlinear inverse problems*, Geophys., 77, W1-W15 (2011).

[8] Groby J.-P., Ogam E., Wirgin A. and Xu Y. *Recovery of a material parameter of a soft elastic layer*, Complex Var.Ellipt.Eqs., 57, 317336 (2012).

[9] Hadamard, J.S., *Lectures on Cauchy's Problem in Linear Partial Differential Equations*, Oxford University Press, Oxford (1923).

[10] Ishida K., *Reconstruction of a layered dielectric cylinder using a split particle swarm optimization*, Proceedings Prog.Electromag.Res. Symposium, Kuala Lumpur, 511-515 (2012).

[11] Kennett B.L.N. and Fichtner A., *A unified concept for comparison of seismograms using transfer functions*, Geophys.J.Int., 191, 1403-1416 (2012).

[12] Kormendi F. and Dietrich M., *Nonlinear waveform inversion of plane-wave seismograms in stratified elastic media*, Geophys., 56, 664-674 (1991).

[13] Lefeuve-Mesgouez G., Mesgouez A., Ogam E., Scotti T. and Wirgin A., *Retrieval of the physical properties of an anelastic solid half space from seismic data*, J.Appl.Geophys., 88, 70-82 (2013).

[14] Le Marrec L., Lasaygues P., Scotti T. and Tsogka C.. *Effcient shape reconstruction of non-circular tubes using broadband acoustic measurements*, Acta Acust., 92, 355-361 (2006).

[15] Ogam E., Fellah Z.E.A. and Baki P., *The inverse problem of acoustic wave scattering by an air-saturated poroelastic cylinder*, J.Acoust.Soc.Am., 133, 1443-1457 (2013).

[16] Pratt R.G., *Inverse theory applied to multi-source cross-hole tomography. Part 2: elastic wave-equation method*, Geophys.Prospect., 38, 311-329 (1990).

[17] Pratt R.G. and Worthington M.H., *Inverse theory applied to multi-source cross-hole tomography. Part 1: acoustic wave-eaution method*, Geophys.Prospect., 38, 287-310 (1990).

[18] Scotti T. and Wirgin A., *Multiparameter identification of a lossy fluid-like object from its transient acoustic response*, Inverse Prob.Sci.Engrg., 22, 1228-1258 (2014).

[19] Sirgue L. and Pratt R.G., *Efficient waveform inversion and imaging: A strategy for selecting temporal frequencies*, Geophys., 69, 231-248 (2004).

[20] Tarantola A., *Inversion of seismic reflection data in the acoustic approximation*, Geophys., 49, 1259-1266 (1984).

[21] Tarantola A., *A strategy for nonlinear elastic inversion of seismic reflection data*, Geophys., 51, 1893-1903 (1986).

[22] Virieux J. and Operto S., *An overview of full-waveform inversion in exploration geophysics*, Geophys., 74, WCC127-WCC152 (2009).

[23] Weglein A., *Roundtable-A timely and ncecessary antidote to indirect methods and so-called P-wave FWI*, The Leading Edge, Oct., 1192-1205 (2013)

[24] Wei Z., *Design of a P-wave seismic vibrator with advanced performance*, GeoArabia, 13, 123-136 (2008).

[25] Wirgin A., *The inverse crime*, http://arxiv.org/abs/math-ph/0401050 (2004).